PHYSICAL REVIEW D **95,** 074028 (2017)

Quark Wigner distributions and spin-spin correlations

D. Chakrabarti,[1] T. Maji,[1] C. Mondal,[1,2] and A. Mukherjee[3]
[1]*Department of Physics, Indian Institute of Technology Kanpur, Kanpur 208016, India*
[2]*Institute of Modern Physics, Chinese Academy of Sciences, Lanzhou 730000, China*
[3]*Department of Physics, Indian Institute of Technology Bombay, Mumbai 400076, India*
(Received 7 February 2017; published 21 April 2017)

We investigate the Wigner distributions for u and d quarks in a light-front quark-diquark model of a proton to unravel the spatial and spin structure. The light-front wave functions are modeled from the soft-wall AdS/QCD prediction. We consider the contributions from both the scalar and the axial vector diquarks. The Wigner distributions for unpolarized, longitudinally polarized, and transversely polarized protons are presented in the transverse momentum plane as well as in the transverse impact parameter plane. The Wigner distributions satisfy a Soffer-bound-type inequality. We also evaluate all the leading-twist GTMDs and show their scale evolution. The spin-spin correlations between the quark and the proton are investigated.

DOI: 10.1103/PhysRevD.95.074028

I. INTRODUCTION

The quark and gluon Wigner distribution introduced by Ji [1,2] have been studied extensively in recent times to understand the three-dimensional structure of the proton. The Wigner distributions encode spatial as well as partonic spin and orbital angular momentum structures. The Wigner distributions are six-dimensional phase-space distributions and are not directly measurable. But after some phase-space reductions, they reduce to the generalized parton distributions (GPDs) and transverse-momentum-dependent distributions (TMDs). The Wigner distributions integrated over transverse momenta reduce to the GPDs at zero skewness, and on integration over the transverse impact parameters with zero momentum transfer, they reduce to the TMDs. It is well known that GPDs and TMDs encode information about the three-dimensional partonic structure of hadrons. Recently, generalized transverse-momentum-dependent PDFs or GTMDs have been introduced [3–5]. Gluon GTMDs have been discussed in Ref. [6]. GTMDs are related to the Wigner distributions, and they again in certain kinematical limits reduce to GPDs and TMDs. The Wigner distributions, after integrating over the light-cone energy of the parton, are interpreted as a Fourier transform of corresponding generalized transverse-momentum-dependent distributions (GTMDs), which are functions of the light-cone three-momentum of the parton as well as the momentum transfer to the nucleon. The spin-spin and spin-orbital angular momentum (OAM) correlations between a nucleon and a quark inside the nucleon can be described from the phase-space average of Wigner distributions. The angular momentum of a quark is extracted from Wigner distributions taking the phase-space average. The Wigner distributions have been studied in different models: e.g. in the light-cone constituent quark model [7–10], the chiral soliton model [8,11,12], the light-front dressed quark model [13–15], the light-cone spectator model [16], and the light-cone quark-scalar-diquark model [17].

In this work, we study the quark Wigner distributions in a light-front quark-diquark model [18] for the proton where the diquark can be either scalar or vector. We have studied the distributions for unpolarized as well as longitudinally and transversely polarized protons. The leading-twist GTMDs are evaluated from the Wigner distributions. The we study the spin and OAM correlations between the quarks and the proton. We find that the quark OAM tends to antialign with the quark spin for u and d quarks but to align with the proton spin.

This paper is organized as follows: We first introduce the light-front quark-diquark model in Sec. II. The Wigner distributions and GTMDs are introduced in Sec. III, and Sec. IV discusses how the OAM spin can be extracted from Wigner distributions and GTMDs. Then, the results in our model are discussed in Sec. V for unpolarized, longitudinally polarized and transversely polarized protons in Secs. V A, V B, and V C, respectively. The spin-spin and spin-OAM correlations are discussed in Sec. V D. A very brief description of the scale evolution of GTMDs is given in Sec. VI. Some inequalities satisfied among the GTMDs and also among the Wigner distributions in our model are shown in Sec. VII. Finally, we conclude the paper with a summary and discussion in Sec. VIII.

II. LIGHT-FRONT QUARK-DIQUARK MODEL FOR NUCLEON

In this model [18], the proton state is written as a superposition of the quark-diquark states allowed under $SU(4)$ spin-flavor symmetry. Thus, the proton can be written as a sum of the isoscalar-scalar diquark singlet state $|uS^0\rangle$, the isoscalar-vector diquark state $|uA^0\rangle$ and the isovector-vector diquark $|dA^1\rangle$ state [19,20], and the state is written as

$$|P;\pm\rangle = C_S|uS^0\rangle^\pm + C_V|uA^0\rangle^\pm + C_{VV}|dA^1\rangle^\pm, \quad (1)$$

where S and A represent the scalar and axial-vector diquarks, with the isospin in their superscripts.

We use the light-cone convention $x^\pm = x^0 \pm x^3$. We choose a frame where the transverse momentum of the proton vanishes, i.e. $P \equiv (P^+, \frac{M^2}{P^+}, \mathbf{0}_\perp)$. In this symmetric frame, the momentum of the struck quark is $p \equiv (xP^+, \frac{p^2+|\mathbf{p}_\perp|^2}{xP^+}, \mathbf{p}_\perp)$, and that of the diquark is $P_X \equiv ((1-x)P^+, P_X^-, -\mathbf{p}_\perp)$. Here $x = p^+/P^+$ is the longitudinal momentum fraction carried by the struck quark. The two-particle Fock-state expansion for $J^z = \pm 1/2$ with a spin-0 diquark is given by

$$|uS\rangle^\pm = \int \frac{dxd^2\mathbf{p}_\perp}{2(2\pi)^3\sqrt{x(1-x)}}\Big[\psi_+^{\pm(u)}(x,\mathbf{p}_\perp)|+\frac{1}{2}s;xP^+,\mathbf{p}_\perp\rangle + \psi_-^{\pm(u)}(x,\mathbf{p}_\perp)|-\frac{1}{2}s;xP^+,\mathbf{p}_\perp\rangle\Big], \quad (2)$$

and the LF wave functions with q spin-0 diquark, for $J = \pm 1/2$, are given by [21]

$$\begin{aligned}
\psi_+^{+(u)}(x,\mathbf{p}_\perp) &= N_S\varphi_1^{(u)}(x,\mathbf{p}_\perp),\\
\psi_-^{+(u)}(x,\mathbf{p}_\perp) &= N_S\left(-\frac{p^1+ip^2}{xM}\right)\varphi_2^{(u)}(x,\mathbf{p}_\perp),\\
\psi_+^{-(u)}(x,\mathbf{p}_\perp) &= N_S\left(\frac{p^1-ip^2}{xM}\right)\varphi_2^{(u)}(x,\mathbf{p}_\perp),\\
\psi_-^{-(u)}(x,\mathbf{p}_\perp) &= N_S\varphi_1^{(u)}(x,\mathbf{p}_\perp),
\end{aligned} \quad (3)$$

where $|\lambda_q\lambda_S;xP^+,\mathbf{p}_\perp\rangle$ is the two-particle state having a struck quark of helicity λ_q and a scalar diquark of helicity $\lambda_S = s$ (the spin-0 singlet diquark helicity is denoted by s to distinguish it from the triplet diquark). The state with a spin-1 diquark is given as [22]

$$\begin{aligned}
|\nu A\rangle^\pm = \int \frac{dxd^2\mathbf{p}_\perp}{2(2\pi)^3\sqrt{x(1-x)}}\Big[&\psi_{++}^{\pm(\nu)}(x,\mathbf{p}_\perp)|+\frac{1}{2}+1;xP^+,\mathbf{p}_\perp\rangle\\
&+\psi_{-+}^{\pm(\nu)}(x,\mathbf{p}_\perp)|-\frac{1}{2}+1;xP^+,\mathbf{p}_\perp\rangle+\psi_{+0}^{\pm(\nu)}(x,\mathbf{p}_\perp)|+\frac{1}{2}0;xP^+,\mathbf{p}_\perp\rangle\\
&+\psi_{-0}^{\pm(\nu)}(x,\mathbf{p}_\perp)|-\frac{1}{2}0;xP^+,\mathbf{p}_\perp\rangle+\psi_{+-}^{\pm(\nu)}(x,\mathbf{p}_\perp)|+\frac{1}{2}-1;xP^+,\mathbf{p}_\perp\rangle\\
&+\psi_{--}^{\pm(\nu)}(x,\mathbf{p}_\perp)|-\frac{1}{2}-1;xP^+,\mathbf{p}_\perp\rangle\Big],
\end{aligned} \quad (4)$$

where $|\lambda_q\lambda_D;xP^+,\mathbf{p}_\perp\rangle$ represents a two-particle state with a quark of helicity $\lambda_q = \pm\frac{1}{2}$ and an axial-vector diquark of helicity $\lambda_D = \pm1, 0$(triplet). The LFWFs are, for $J = +1/2$

$$\begin{aligned}
\psi_{++}^{+(\nu)}(x,\mathbf{p}_\perp) &= N_1^{(\nu)}\sqrt{\frac{2}{3}}\left(\frac{p^1-ip^2}{xM}\right)\varphi_2^{(\nu)}(x,\mathbf{p}_\perp),\\
\psi_{-+}^{+(\nu)}(x,\mathbf{p}_\perp) &= N_1^{(\nu)}\sqrt{\frac{2}{3}}\varphi_1^{(\nu)}(x,\mathbf{p}_\perp),\\
\psi_{+0}^{+(\nu)}(x,\mathbf{p}_\perp) &= -N_0^{(\nu)}\sqrt{\frac{1}{3}}\varphi_1^{(\nu)}(x,\mathbf{p}_\perp),\\
\psi_{-0}^{+(\nu)}(x,\mathbf{p}_\perp) &= N_0^{(\nu)}\sqrt{\frac{1}{3}}\left(\frac{p^1+ip^2}{xM}\right)\varphi_2^{(\nu)}(x,\mathbf{p}_\perp),\\
\psi_{+-}^{+(\nu)}(x,\mathbf{p}_\perp) &= 0,\\
\psi_{--}^{+(\nu)}(x,\mathbf{p}_\perp) &= 0,
\end{aligned} \quad (5)$$

and for $J = -1/2$

$$\begin{aligned}
\psi_{++}^{-(\nu)}(x,\mathbf{p}_\perp) &= 0,\\
\psi_{-+}^{-(\nu)}(x,\mathbf{p}_\perp) &= 0,\\
\psi_{+0}^{-(\nu)}(x,\mathbf{p}_\perp) &= N_0^{(\nu)}\sqrt{\frac{1}{3}}\left(\frac{p^1-ip^2}{xM}\right)\varphi_2^{(\nu)}(x,\mathbf{p}_\perp),\\
\psi_{-0}^{-(\nu)}(x,\mathbf{p}_\perp) &= N_0^{(\nu)}\sqrt{\frac{1}{3}}\varphi_1^{(\nu)}(x,\mathbf{p}_\perp),\\
\psi_{+-}^{-(\nu)}(x,\mathbf{p}_\perp) &= -N_1^{(\nu)}\sqrt{\frac{2}{3}}\varphi_1^{(\nu)}(x,\mathbf{p}_\perp),\\
\psi_{--}^{-(\nu)}(x,\mathbf{p}_\perp) &= N_1^{(\nu)}\sqrt{\frac{2}{3}}\left(\frac{p^1+ip^2}{xM}\right)\varphi_2^{(\nu)}(x,\mathbf{p}_\perp),
\end{aligned} \quad (6)$$

having flavor index $\nu = u, d$. The LFWFs $\varphi_i^{(\nu)}(x,\mathbf{p}_\perp)$ are a modified form of the soft-wall AdS/QCD prediction

$$\varphi_i^{(\nu)}(x,\mathbf{p}_\perp) = \frac{4\pi}{\kappa}\sqrt{\frac{\log(1/x)}{1-x}}x^{a_i^\nu}(1-x)^{b_i^\nu} \times \exp\left[-\delta^\nu\frac{\mathbf{p}_\perp^2}{2\kappa^2}\frac{\log(1/x)}{(1-x)^2}\right]. \quad (7)$$

The wave functions $\varphi_i^\nu (i = 1, 2)$ reduce to the AdS/QCD prediction [23,24] for the parameters $a_i^\nu = b_i^\nu = 0$ and $\delta^\nu = 1.0$. We use the AdS/QCD scale parameter $\kappa = 0.4$ GeV as determined in Ref. [25], and the quarks are assumed to be massless.

III. WIGNER DISTRIBUTIONS

In the same way as the impact-parameter-dependent parton distributions (IPDs) are obtained by the two-dimensional Fourier transforms of the generalized parton distributions (GPDs), one can map out the Wigner distributions as the two-dimensional Fourier transforms of the so-called generalized transverse-momentum-dependent parton distributions (GTMDs). In the light-front framework, one defines the five-dimensional quark Wigner distributions as [7,8]

$$\rho^{\nu[\Gamma]}(\mathbf{b}_\perp, \mathbf{p}_\perp, x; S) = \int \frac{d^2\Delta_\perp}{(2\pi)^2} e^{-i\Delta_\perp . b_\perp} W^{\nu[\Gamma]}(\mathbf{\Delta}_\perp, \mathbf{p}_\perp, x; S). \tag{8}$$

The correlator $W^{[\Gamma]}$ relates the GTMDs [3,4], and in the Drell-Yan-West frame ($\Delta^+ = 0$) and fixed light-cone time $z^+ = 0$, it is given by

$$W^{\nu[\Gamma]}(\mathbf{\Delta}_\perp, \mathbf{p}_\perp, x; S) = \frac{1}{2}\int \frac{dz^-}{(2\pi)}\frac{d^2z_T}{(2\pi)^2} e^{ip.z}\langle P''; S|\bar{\psi}_i^\nu(-z/2)\Gamma\mathcal{W}_{[-z/2,z/2]}\psi_j^\nu(z/2)|P'; S\rangle|_{z^+=0}. \tag{9}$$

The Γ denotes the twist-2 Dirac γ-matrices $\gamma^+, \gamma^+\gamma^5$ and $i\sigma^{j+}\gamma^5$ (with $j = 1, 2$) corresponding to unpolarized, longitudinally polarized and transversely polarized quarks respectively. The gauge link Wilson line, $\mathcal{W}_{[-z/2,z/2]}$, ensures the $SU(3)$ color gauge invariance of the Wigner operator. $P'(P'')$ and S represent the proton momentum of the initial (final) state of the proton and the spin of the proton state, respectively. We use the light-front coordinates $v^\mu = [v^+, v^-, \vec{v}_\perp]$, where $v^\pm = (v^0 \pm v^3)$ and $\vec{v}_\perp = (v^1, v^2)$. The kinematical variables are defined as

$$P^\mu = \frac{(P' + P'')^\mu}{2}, \qquad \Delta^\mu = (P'' - P')^\mu. \tag{10}$$

Depending on the various polarization configurations of the proton and the quark, there are 16 independent twist-2 quark Wigner distributions. In an unpolarized proton, the quark Wigner distributions for unpolarized, longitudinally polarized, and transversely polarized quarks are defined as [8,26]

$$\rho_{UU}^\nu(\mathbf{b}_\perp, \mathbf{p}_\perp, x) = \frac{1}{2}[\rho^{\nu[\gamma^+]}(\mathbf{b}_\perp, \mathbf{p}_\perp, x; +\hat{S}_z) + \rho^{\nu[\gamma^+]}(\mathbf{b}_\perp, \mathbf{p}_\perp, x; -\hat{S}_z)], \tag{11}$$

$$\rho_{UL}^\nu(\mathbf{b}_\perp, \mathbf{p}_\perp, x) = \frac{1}{2}[\rho^{\nu[\gamma^+\gamma^5]}(\mathbf{b}_\perp, \mathbf{p}_\perp, x; +\hat{S}_z) + \rho^{\nu[\gamma^+\gamma^5]}(\mathbf{b}_\perp, \mathbf{p}_\perp, x; -\hat{S}_z)], \tag{12}$$

$$\rho_{UT}^{\nu j}(\mathbf{b}_\perp, \mathbf{p}_\perp, x) = \frac{1}{2}[\rho^{\nu[i\sigma^{j+}\gamma^5]}(\mathbf{b}_\perp, \mathbf{p}_\perp, x; +\hat{S}_z) + \rho^{\nu[i\sigma^{j+}\gamma^5]}(\mathbf{b}_\perp, \mathbf{p}_\perp, x; -\hat{S}_z)]. \tag{13}$$

For a longitudinally polarized proton and different polarizations of the quark, the distributions are given by

$$\rho_{LU}^\nu(\mathbf{b}_\perp, \mathbf{p}_\perp, x) = \frac{1}{2}[\rho^{\nu[\gamma^+]}(\mathbf{b}_\perp, \mathbf{p}_\perp, x; +\hat{S}_z) - \rho^{\nu[\gamma^+]}(\mathbf{b}_\perp, \mathbf{p}_\perp, x; -\hat{S}_z)], \tag{14}$$

$$\rho_{LL}^\nu(\mathbf{b}_\perp, \mathbf{p}_\perp, x) = \frac{1}{2}[\rho^{\nu[\gamma^+\gamma^5]}(\mathbf{b}_\perp, \mathbf{p}_\perp, x; +\hat{S}_z) - \rho^{\nu[\gamma^+\gamma^5]}(\mathbf{b}_\perp, \mathbf{p}_\perp, x; -\hat{S}_z)], \tag{15}$$

$$\rho_{LT}^{\nu j}(\mathbf{b}_\perp, \mathbf{p}_\perp, x) = \frac{1}{2}[\rho^{\nu[i\sigma^{j+}\gamma^5]}(\mathbf{b}_\perp, \mathbf{p}_\perp, x; +\hat{S}_z) - \rho^{\nu[i\sigma^{j+}\gamma^5]}(\mathbf{b}_\perp, \mathbf{p}_\perp, x; -\hat{S}_z)]. \tag{16}$$

Again, the Wigner distributions for a transversely polarized proton with various quark polarizations are identified as

$$\rho_{TU}^{i\nu}(\mathbf{b}_\perp, \mathbf{p}_\perp, x) = \frac{1}{2}[\rho^{\nu[\gamma^+]}(\mathbf{b}_\perp, \mathbf{p}_\perp, x; +\hat{S}_i) - \rho^{\nu[\gamma^+]}(\mathbf{b}_\perp, \mathbf{p}_\perp, x; -\hat{S}_i)], \tag{17}$$

$$\rho_{TL}^{i\nu}(\mathbf{b}_\perp, \mathbf{p}_\perp, x) = \frac{1}{2}[\rho^{\nu[\gamma^+\gamma^5]}(\mathbf{b}_\perp, \mathbf{p}_\perp, x; +\hat{S}_i) - \rho^{\nu[\gamma^+\gamma^5]}(\mathbf{b}_\perp, \mathbf{p}_\perp, x; -\hat{S}_i)], \tag{18}$$

$$\rho^{\nu}_{TT}(\mathbf{b}_\perp,\mathbf{p}_\perp,x)=\frac{1}{2}\delta_{ij}[\rho^{\nu[i\sigma^{j+}\gamma^5]}(\mathbf{b}_\perp,\mathbf{p}_\perp,x;+\hat{S}_i)-\rho^{\nu[i\sigma^{j+}\gamma^5]}(\mathbf{b}_\perp,\mathbf{p}_\perp,x;-\hat{S}_i)], \tag{19}$$

and the pretzelous Wigner distribution is defined as

$$\rho^{\nu\perp}_{TT}(\mathbf{b}_\perp,\mathbf{p}_\perp,x)=\frac{1}{2}\epsilon_{ij}[\rho^{\nu[i\sigma^{j+}\gamma^5]}(\mathbf{b}_\perp,\mathbf{p}_\perp,x;+\hat{S}_i)-\rho^{\nu[i\sigma^{j+}\gamma^5]}(\mathbf{b}_\perp,\mathbf{p}_\perp,x;-\hat{S}_i)]. \tag{20}$$

Here the first subscript denotes the proton polarization, and the second one represents the quark polarization. The Wigner distributions are directly connected to the generalized parton correlation functions [3,8]. At $z_{\perp=0}$, integrating over momentum $\mathbf{p}_\perp$, the Wigner distributions reduce to impact-parameter-dependent parton distributions (IPDs) which can be interpreted as quark densities in the transverse position space. Again, the $\mathbf{b}_\perp$ integration of the distributions gives the transverse-momentum-dependent parton distributions (TMDs), which can be interpreted as quark densities in transverse momentum space. In the Drell-Yan-West frame, the Wigner distributions may have a quasiprobability interpretation [8], but the interpretation is lost when one defines a six-dimensional Wigner distribution, $\rho^{\nu[\Gamma]}(\mathbf{b}_\perp,\xi,\mathbf{p}_\perp,x;\hat{S})$, by including a longitudinal momentum transfer [$\xi=-\Delta^+/(2P^+)$]. One can also obtain the three-dimensional quark densities by integrating over two mutually orthogonal components of transverse position and momentum, e.g. b_y and p_x (b_x and p_y), which are not constrained by the Heisenberg uncertainty principle, as [8]

$$\int db_y dp_x \rho^{\nu[\Gamma]}(\mathbf{b}_\perp,\mathbf{p}_\perp,x;S)=\tilde{\rho}^{\nu[\Gamma]}(b_x,p_y,x;S) \tag{21}$$

with $\Delta_y=z_x=0$ and

$$\int db_x dp_y \rho^{\nu[\Gamma]}(\mathbf{b}_\perp,\mathbf{p}_\perp,x;S)=\bar{\rho}^{\nu[\Gamma]}(b_y,p_x,x;S) \tag{22}$$

with $\Delta_x=z_y=0$. For unpolarized and longitudinally polarized protons, the distributions $\tilde{\rho}^{\nu[\Gamma]}(b_y,p_x,x;S)$ and $\bar{\rho}^{\nu[\Gamma]}(b_x,-p_y,x;S)$ are same. The Wigner distribution of quarks with longitudinal polarization λ in a longitudinally polarized proton Λ is defined for $\Gamma=\gamma^+\frac{\mathbb{1}+\lambda\gamma^5}{2}$ and $\vec{S}=\Lambda\hat{S}_z$ as [8]

$$\rho^{\nu}_{\Lambda\lambda}(\mathbf{b}_\perp,\mathbf{p}_\perp,x)=\frac{1}{2}[\rho^{\nu[\gamma^+]}(\mathbf{b}_\perp,\mathbf{p}_\perp,x;\Lambda\hat{S}_z)+\lambda\rho^{\nu[\gamma^+\gamma^5]}(\mathbf{b}_\perp,\mathbf{p}_\perp,x;\Lambda\hat{S}_z)], \tag{23}$$

which can be decomposed as

$$\rho^{\nu}_{\Lambda\lambda}(\mathbf{b}_\perp,\mathbf{p}_\perp,x)=\frac{1}{2}[\rho^{\nu}_{UU}(\mathbf{b}_\perp,\mathbf{p}_\perp,x)+\Lambda\rho^{\nu}_{LU}(\mathbf{b}_\perp,\mathbf{p}_\perp,x)+\lambda\rho^{\nu}_{UL}(\mathbf{b}_\perp,\mathbf{p}_\perp,x)+\Lambda\lambda\rho^{\nu}_{LL}(\mathbf{b}_\perp,\mathbf{p}_\perp,x)], \tag{24}$$

corresponding to $\Lambda=\uparrow,\downarrow$ and $\lambda=\uparrow,\downarrow$ (where $\uparrow$ and $\downarrow$ correspond to $+1$ and -1, respectively, for longitudinal polarizations). Similarly, the Wigner distribution for a quark with transverse polarizations $\lambda_T=\Uparrow,\Downarrow$ in a proton with transverse polarizations $\Lambda_T=\Uparrow,\Downarrow$ can be written as

$$\rho^{i\nu}_{\Lambda_T\lambda_T}(\mathbf{b}_\perp,\mathbf{p}_\perp,x)=\frac{1}{2}[\rho^{\nu[\gamma^+]}(\mathbf{b}_\perp,\mathbf{p}_\perp,x;\Lambda_T\hat{S}_i)+\Lambda_T\rho^{\nu[i\sigma^{i+}\gamma^5]}(\mathbf{b}_\perp,\mathbf{p}_\perp,x;\Lambda_T\hat{S}_i)], \tag{25}$$

which can be decomposed as

$$\rho^{i\nu}_{\Lambda_T\lambda_T}(\mathbf{b}_\perp,\mathbf{p}_\perp,x)=\frac{1}{2}[\rho^{\nu}_{UU}(\mathbf{b}_\perp,\mathbf{p}_\perp,x)+\Lambda_T\rho^{i\nu}_{TU}(\mathbf{b}_\perp,\mathbf{p}_\perp,x)+\lambda_T\rho^{\nu i}_{UT}(\mathbf{b}_\perp,\mathbf{p}_\perp,x)+\Lambda_T\lambda_T\rho^{q}_{TT}(\mathbf{b}_\perp,\mathbf{p}_\perp,x)]. \tag{26}$$

The distribution $\rho^{\nu}_{\Lambda\lambda}(\mathbf{b}_\perp,\mathbf{p}_\perp,x)$ in the transverse plane is shown in Figs. 12 and 13 for u and d quarks, respectively. The transverse Wigner distribution $\rho^{i\nu}_{\Lambda_T\lambda_T}(\mathbf{b}_\perp,\mathbf{p}_\perp,x)$ is shown in Figs. 14 and 15 with $i=1$ (i.e. polarization along the x-axis). $\rho^{\nu}_{\Lambda\lambda}(\mathbf{b}_\perp,\mathbf{p}_\perp,x)$ and $\rho^{i\nu}_{\Lambda_T\lambda_T}(\mathbf{b}_\perp,\mathbf{p}_\perp,x)$ provide information about the correlations between proton spin and quark spin in the longitudinal direction and in the transverse direction, respectively. We also can define the Wigner distributions for longitudinally polarized quarks in a transversely polarized proton $\rho^{i\nu}_{\Lambda_T\lambda}(\mathbf{b}_\perp,\mathbf{p}_\perp,x)$, and for transversely polarized quarks in a longitudinally polarized proton $\rho^{\nu j}_{\Lambda\lambda_T}(\mathbf{b}_\perp,\mathbf{p}_\perp,x)$, as

$$\rho^{i\nu}_{\Lambda_T\lambda}(\mathbf{b}_\perp,\mathbf{p}_\perp,x)=\frac{1}{2}[\rho^{\nu}_{UU}(\mathbf{b}_\perp,\mathbf{p}_\perp,x)+\Lambda_T\rho^{i\nu}_{TU}(\mathbf{b}_\perp,\mathbf{p}_\perp,x)+\lambda\rho^{\nu}_{UL}(\mathbf{b}_\perp,\mathbf{p}_\perp,x)+\Lambda_T\lambda\rho^{i\nu}_{TL}(\mathbf{b}_\perp,\mathbf{p}_\perp,x)], \tag{27}$$

$$\rho^{\nu j}_{\Lambda\lambda_T}(\mathbf{b}_\perp,\mathbf{p}_\perp,x)=\frac{1}{2}[\rho^{\nu}_{UU}(\mathbf{b}_\perp,\mathbf{p}_\perp,x)+\Lambda\rho^{\nu}_{LU}(\mathbf{b}_\perp,\mathbf{p}_\perp,x)+\lambda_T\rho^{\nu j}_{UT}(\mathbf{b}_\perp,\mathbf{p}_\perp,x)+\Lambda\lambda_T\rho^{\nu j}_{LT}(\mathbf{b}_\perp,\mathbf{p}_\perp,x)]. \tag{28}$$

The Wigner correlator, Eq. (8), can be parametrized in terms of GTMDs [4]

(i) for unpolarized protons as

$$\rho^{\nu}_{UU}(\mathbf{b}_\perp,\mathbf{p}_\perp,x)=\mathcal{F}^{\nu}_{1,1}(x,0,\mathbf{p}^2_\perp,\mathbf{p}_\perp.\mathbf{b}_\perp,\mathbf{b}^2_\perp), \tag{29}$$

$$\rho^{\nu}_{UL}(\mathbf{b}_\perp,\mathbf{p}_\perp,x)=\frac{1}{M^2}\epsilon^{ij}_\perp p^i_\perp\frac{\partial}{\partial b^j_\perp}\mathcal{G}^{\nu}_{1,1}(x,0,\mathbf{p}^2_\perp,\mathbf{p}_\perp.\mathbf{b}_\perp,\mathbf{b}^2_\perp), \tag{30}$$

$$\rho^{\nu j}_{UT}(\mathbf{b}_\perp,\mathbf{p}_\perp,x)=-i\frac{1}{M}\epsilon^{ij}_\perp p^i_\perp\mathcal{H}^{\nu}_{1,1}(x,0,\mathbf{p}^2_\perp,\mathbf{p}_\perp.\mathbf{b}_\perp,\mathbf{b}^2_\perp)+\frac{1}{M}\epsilon^{ij}_\perp\frac{\partial}{\partial b^i_\perp}\mathcal{H}^{\nu}_{1,2}(x,0,\mathbf{p}^2_\perp,\mathbf{p}_\perp.\mathbf{b}_\perp,\mathbf{b}^2_\perp); \tag{31}$$

(ii) for longitudinally polarized protons as

$$\rho^{\nu}_{LU}(\mathbf{b}_\perp,\mathbf{p}_\perp,x)=-\frac{1}{M^2}\epsilon^{ij}_\perp p^i_\perp\frac{\partial}{\partial b^j_\perp}\mathcal{F}^{\nu}_{1,4}(x,0,\mathbf{p}^2_\perp,\mathbf{p}_\perp.\mathbf{b}_\perp,\mathbf{b}^2_\perp), \tag{32}$$

$$\rho^{\nu}_{LL}(\mathbf{b}_\perp,\mathbf{p}_\perp,x)=\mathcal{G}^{\nu}_{1,4}(x,0,\mathbf{p}^2_\perp,\mathbf{p}_\perp.\mathbf{b}_\perp,\mathbf{b}^2_\perp), \tag{33}$$

$$\rho^{\nu j}_{LT}(\mathbf{b}_\perp,\mathbf{p}_\perp,x)=\frac{p^j_\perp}{M}\mathcal{H}^{\nu}_{1,7}(x,0,\mathbf{p}^2_\perp,\mathbf{p}_\perp.\mathbf{b}_\perp,\mathbf{b}^2_\perp)+i\frac{1}{M}\frac{\partial}{\partial b^j_\perp}\mathcal{H}^{\nu}_{1,8}(x,0,\mathbf{p}^2_\perp,\mathbf{p}_\perp.\mathbf{b}_\perp,\mathbf{b}^2_\perp); \tag{34}$$

(iii) and for transversely polarized protons as

$$\begin{aligned}\rho^{i\nu}_{TU}(\mathbf{b}_\perp,\mathbf{p}_\perp,x)=&\frac{1}{2M}\epsilon^{ij}_\perp\frac{\partial}{\partial b^j_\perp}[\mathcal{F}^{\nu}_{1,1}(x,0,\mathbf{p}^2_\perp,\mathbf{p}_\perp.\mathbf{b}_\perp,\mathbf{b}^2_\perp)-2\mathcal{F}^{\nu}_{1,3}(x,0,\mathbf{p}^2_\perp,\mathbf{p}_\perp.\mathbf{b}_\perp,\mathbf{b}^2_\perp)]\\&+i\frac{1}{M}\epsilon^{ij}_\perp p^j_\perp\mathcal{F}^{\nu}_{1,2}(x,0,\mathbf{p}^2_\perp,\mathbf{p}_\perp.\mathbf{b}_\perp,\mathbf{b}^2_\perp),\end{aligned} \tag{35}$$

$$\begin{aligned}\rho^{i\nu}_{TL}(\mathbf{b}_\perp,\mathbf{p}_\perp,x)=&\frac{1}{2M^3}\epsilon^{ij}_\perp\epsilon^{kl}_\perp p^k_\perp\frac{\partial}{\partial b^j_\perp}\frac{\partial}{\partial b^l_\perp}\mathcal{G}_{1,1}(x,0,\mathbf{p}^2_\perp,\mathbf{p}_\perp.\mathbf{b}_\perp,\mathbf{b}^2_\perp)\\&+\frac{p^i_\perp}{M}\mathcal{G}^{\nu}_{1,2}(x,0,\mathbf{p}^2_\perp,\mathbf{p}_\perp.\mathbf{b}_\perp,\mathbf{b}^2_\perp)+i\frac{1}{M}\frac{\partial}{\partial b^i_\perp}\mathcal{G}^{\nu}_{1,3}(x,0,\mathbf{p}^2_\perp,\mathbf{p}_\perp.\mathbf{b}_\perp,\mathbf{b}^2_\perp),\end{aligned} \tag{36}$$

$$\begin{aligned}\rho^{\nu}_{TT}(\mathbf{b}_\perp,\mathbf{p}_\perp,x)=&\epsilon^{ij}(-1)^i\left[-i\frac{p^j_\perp}{2M^2}\frac{\partial}{\partial b^j_\perp}\mathcal{H}_{1,1}(x,0,\mathbf{p}^2_\perp,\mathbf{p}_\perp.\mathbf{b}_\perp,\mathbf{b}^2_\perp)+\frac{1}{2M^2}\frac{\partial^2}{\partial b^{j2}_\perp}\mathcal{H}_{1,2}(x,0,\mathbf{p}^2_\perp,\mathbf{p}_\perp.\mathbf{b}_\perp,\mathbf{b}^2_\perp)\right]\\&+\mathcal{H}^{\nu}_{1,3}(x,0,\mathbf{p}^2_\perp,\mathbf{p}_\perp.\mathbf{b}_\perp,\mathbf{b}^2_\perp)+\delta_{ij}\left[\frac{p^i_\perp p^j_\perp}{M^2}\mathcal{H}^{\nu}_{1,4}(x,0,\mathbf{p}^2_\perp,\mathbf{p}_\perp.\mathbf{b}_\perp,\mathbf{b}^2_\perp)\right.\\&\left.+\frac{1}{M^2}p^i_\perp\frac{\partial}{\partial b^j_\perp}\mathcal{H}^{\nu}_{1,5}(x,0,\mathbf{p}^2_\perp,\mathbf{p}_\perp.\mathbf{b}_\perp,\mathbf{b}^2_\perp)-\frac{1}{M^2}\frac{\partial}{\partial b^i_\perp}\frac{\partial}{\partial b^j_\perp}\mathcal{H}^{\nu}_{1,6}(x,0,\mathbf{p}^2_\perp,\mathbf{p}_\perp.\mathbf{b}_\perp,\mathbf{b}^2_\perp)\right].\end{aligned} \tag{37}$$

The pretzelous distribution is parametrized as

$$\begin{aligned}\rho^{\perp\nu}_{TT}(\mathbf{b}_\perp,\mathbf{p}_\perp,x)=&\frac{\epsilon^{ij}_\perp}{2M^2}\left[ip^i\frac{\partial}{\partial b^j_\perp}(-\mathcal{H}^{\nu}_{1,1}(x,0,\mathbf{p}^2_\perp,\mathbf{p}_\perp.\mathbf{b}_\perp,\mathbf{b}^2_\perp)+2\mathcal{H}^{\nu}_{1,5}(x,0,\mathbf{p}^2_\perp,\mathbf{p}_\perp.\mathbf{b}_\perp,\mathbf{b}^2_\perp))\right.\\&+\frac{\partial}{\partial b^i_\perp}\frac{\partial}{\partial b^j_\perp}(\mathcal{H}^{\nu}_{1,2}(x,0,\mathbf{p}^2_\perp,\mathbf{p}_\perp.\mathbf{b}_\perp,\mathbf{b}^2_\perp)-2\mathcal{H}^{\nu}_{1,6}(x,0,\mathbf{p}^2_\perp,\mathbf{p}_\perp.\mathbf{b}_\perp,\mathbf{b}^2_\perp))\\&\left.+2p^ip^j\mathcal{H}^{\nu}_{1,4}(x,0,\mathbf{p}^2_\perp,\mathbf{p}_\perp.\mathbf{b}_\perp,\mathbf{b}^2_\perp)\right],\end{aligned} \tag{38}$$

where $\chi^\nu=\mathcal{F}^{\nu}_{1,1},\mathcal{F}^{\nu}_{1,4},\mathcal{G}^{\nu}_{1,1},\mathcal{G}^{\nu}_{1,4}$, and $\mathcal{H}_{1,n}$ $(n=1,2,3\ldots8)$ can be expressed as the Fourier transforms of the GTMDs $X^\nu=F^{\nu}_{1,1},F^{\nu}_{1,4},G^{\nu}_{1,1},G^{\nu}_{1,4}$, and $H_{1,n}$, respectively:

$$\chi^{\nu}(x,0,\mathbf{p}_\perp^2,\mathbf{p}_\perp.\mathbf{b}_\perp,\mathbf{b}_\perp^2) = \int \frac{d^2\Delta_\perp}{(2\pi)^2} e^{-i\Delta_\perp.\mathbf{b}_\perp} X^{\nu}(x,0,\mathbf{p}_\perp^2,\mathbf{p}_\perp.\mathbf{\Delta}_\perp,\mathbf{\Delta}_\perp^2). \quad (39)$$

There are altogether 16 GTMDs at the leading twist. At $\Delta = 0$, the GTMDs reduce to transverse-momentum-dependent distributions (TMDs), which are functions of the longitudinal momentum fraction x and transverse momentum $\mathbf{p}_\perp$ carried by the quark. There are altogether eight TMDs at the leading twist.

IV. ORBITAL ANGULAR MOMENTUM

The canonical orbital angular momentum (OAM) operator for the quark is defined as

$$\hat{\ell}_z^{\nu}(b^-,\mathbf{b}_\perp,p^+,\mathbf{p}_\perp) = \frac{1}{4}\int \frac{dz^- d^2\mathbf{z}_\perp}{(2\pi)^3} e^{-ip.z}\bar{\psi}^{\nu}(b^-,\mathbf{b}_\perp)\gamma^+(\mathbf{b}_\perp\times(-i\partial_\perp))\psi^{\nu}(b^- - z^-,\mathbf{b}_\perp). \quad (40)$$

The OAM density operator can be expressed in terms of the Wigner operator as

$$\hat{\ell}_z^{\nu} = (\mathbf{b}_\perp\times\mathbf{p}_\perp)\hat{W}^{\nu[\gamma^+]}. \quad (41)$$

Thus, in light-front gauge, the average canonical OAM for the quark is written in terms of Wigner distribution as

$$\ell_z^{\nu} = \int \frac{d\Delta^+ d^2\Delta_\perp}{2P^+(2\pi)^3}\langle P'';S|\hat{\ell}_z^{\nu}|P';S\rangle = \int dx d^2\mathbf{p}_\perp d^2\mathbf{b}_\perp (\mathbf{b}_\perp\times\mathbf{p}_\perp)_z \rho^{\nu[\gamma^+]}(\mathbf{b}_\perp,\mathbf{p}_\perp,x,\hat{S}_z), \quad (42)$$

where the distribution $\rho^{\nu[\gamma^+]}(\mathbf{b}_\perp,\mathbf{p}_\perp,x,\hat{S}_z)$ can be written from Eqs. (11) and (14) as

$$\rho^{\nu[\gamma^+]}(\mathbf{b}_\perp,\mathbf{p}_\perp,x,+\hat{S}_z) = \rho^{\nu}_{UU}(\mathbf{b}_\perp,\mathbf{p}_\perp,x) + \rho^{\nu}_{LU}(\mathbf{b}_\perp,\mathbf{p}_\perp,x). \quad (43)$$

From Eq. (29), we see that

$$\int dx d^2\mathbf{p}_\perp d^2\mathbf{b}_\perp (\mathbf{b}_\perp\times\mathbf{p}_\perp)_z \rho^{\nu}_{UU}(\mathbf{b}_\perp,\mathbf{p}_\perp,x) = 0, \quad (44)$$

which satisfies the angular momentum sum rule for unpolarized protons—the total angular momentum of the constituents sums up to zero. From Eqs. (32) and (39), the twist-2 canonical quark OAM in the light-front gauge is written in terms of the GTMDs as

$$\ell_z^{\nu} = -\int dx d^2\mathbf{p}_\perp \frac{\mathbf{p}_\perp^2}{M^2} F^{\nu}_{1,4}(x,0,\mathbf{p}_\perp^2,0,0). \quad (45)$$

The correlation between proton spin and quark OAM is understood from ℓ_z^{ν}. If $\ell_z^{\nu} > 0$, the quark OAM is parallel to the proton spin, and $\ell_z^{\nu} < 0$ indicates that the quark OAM is antiparallel to the proton spin.

The spin-orbit correlation of a quark is given by the operator

$$C_z^{\nu}(b^-,\mathbf{b}_\perp,p^+,\mathbf{p}_\perp) = \frac{1}{4}\int \frac{dz^- d^2\mathbf{z}_\perp}{(2\pi)^3} e^{-ip.z}\bar{\psi}^{\nu}(b^-,\mathbf{b}_\perp)\gamma^+\gamma^5(\mathbf{b}_\perp\times(-i\partial_\perp))\psi^{\nu}(b^- - z^-,\mathbf{b}_\perp). \quad (46)$$

The correlation between quark spin and quark OAM can be expressed with Wigner distributions ρ^{ν}_{UL}, and equivalently in terms of GTMD as

$$C_z^{\nu} = \int dx d^2\mathbf{p}_\perp d^2\mathbf{b}_\perp (\mathbf{b}_\perp\times\mathbf{p}_\perp)_z \rho^{\nu}_{UL}(\mathbf{b}_\perp,\mathbf{p}_\perp,x) = \int dx d^2\mathbf{p}_\perp \frac{\mathbf{p}_\perp^2}{M^2} G^{\nu}_{1,1}(x,0,\mathbf{p}_\perp^2,0,0), \quad (47)$$

where $C_z^{\nu} > 0$ implies that the quark spin and OAM tend to be aligned and $C_z^{\nu} < 0$ implies that they are antialigned.

The spin contribution of the quark to the proton spin is defined [8] as

$$s_z^{\nu} = \frac{1}{2}g_A^{\nu} = \frac{1}{2}\int dx \tilde{H}^{\nu}(x,0,0) = \frac{1}{2}\int dx d^2p_\perp G^{\nu}_{1,4}(x,0,\mathbf{p}_\perp^2,0,0), \quad (48)$$

where g_A^{ν} is the axial charge.

V. RESULTS

The quark Wigner distributions are evaluated in the light-front quark-diquark model constructed from the AdS/QCD correspondence. Using the two-particle Fock states expression of the proton for both the scalar and vector diquarks in Eq. (9), we can express the quark-quark correlator $W^{\nu[\Gamma]}(\mathbf{\Delta}_\perp,\mathbf{p}_\perp,x;S)$ in terms of LFWFs. For the scalar diquark, the expansion of $W^{\nu[\Gamma]}(\mathbf{\Delta}_\perp,\mathbf{p}_\perp,x;S)$ is given by

$$W_S^{\nu[\gamma^+]}(\boldsymbol{\Delta}_\perp,\mathbf{p}_\perp,x;\pm\hat{S}_z)=\frac{1}{16\pi^3}[\psi_{\nu+}^{\pm\dagger}(x,\mathbf{p}''_\perp)\psi_{\nu+}^{\pm}(x,\mathbf{p}'_\perp)+\psi_{\nu-}^{\pm\dagger}(x,\mathbf{p}''_\perp)\psi_{\nu-}^{\pm}(x,\mathbf{p}'_\perp)], \tag{49}$$

$$W_S^{\nu[\gamma^+\gamma^5]}(\boldsymbol{\Delta}_\perp,\mathbf{p}_\perp,x;\pm\hat{S}_z)=\frac{1}{16\pi^3}[\psi_{\nu+}^{\pm\dagger}(x,\mathbf{p}''_\perp)\psi_{\nu+}^{\pm}(x,\mathbf{p}'_\perp)-\psi_{\nu-}^{\pm\dagger}(x,\mathbf{p}''_\perp)\psi_{\nu-}^{\pm}(x,\mathbf{p}'_\perp)], \tag{50}$$

$$W_S^{\nu[i\sigma^{j+}\gamma^5]}(\boldsymbol{\Delta}_\perp,\mathbf{p}_\perp,x;\pm\hat{S}_z)=\frac{1}{16\pi^3}\epsilon_\perp^{ij}[(-i)^i\psi_{\nu+}^{\pm\dagger}(x,\mathbf{p}''_\perp)\psi_{\nu-}^{\pm}(x,\mathbf{p}'_\perp)+(i)^i\psi_{\nu-}^{\pm\dagger}(x,\mathbf{p}''_\perp)\psi_{\nu+}^{\pm}(x,\mathbf{p}'_\perp)]. \tag{51}$$

For the vector diquark, the expressions read as

$$\begin{aligned}W_A^{\nu[\gamma^+]}(\boldsymbol{\Delta}_\perp,\mathbf{p}_\perp,x;\pm\hat{S}_z)=\frac{1}{16\pi^3}[&\psi_{\nu++}^{\pm\dagger}(x,\mathbf{p}''_\perp)\psi_{\nu++}^{\pm}(x,\mathbf{p}'_\perp)+\psi_{\nu-+}^{\pm\dagger}(x,\mathbf{p}''_\perp)\psi_{\nu-+}^{\pm}(x,\mathbf{p}'_\perp)\\&+\psi_{\nu+0}^{\pm\dagger}(x,\mathbf{p}''_\perp)\psi_{\nu+0}^{\pm}(x,\mathbf{p}'_\perp)+\psi_{\nu-0}^{\pm\dagger}(x,\mathbf{p}''_\perp)\psi_{\nu-0}^{\pm}(x,\mathbf{p}'_\perp)\\&+\psi_{\nu+-}^{\pm\dagger}(x,\mathbf{p}''_\perp)\psi_{\nu+-}^{\pm}(x,\mathbf{p}'_\perp)+\psi_{\nu--}^{\pm\dagger}(x,\mathbf{p}''_\perp)\psi_{\nu--}^{\pm}(x,\mathbf{p}'_\perp)],\end{aligned} \tag{52}$$

$$\begin{aligned}W_A^{\nu[\gamma^+\gamma^5]}(\boldsymbol{\Delta}_\perp,\mathbf{p}_\perp,x;\pm\hat{S}_z)=\frac{1}{16\pi^3}[&\psi_{\nu++}^{\pm\dagger}(x,\mathbf{p}''_\perp)\psi_{\nu++}^{\pm}(x,\mathbf{p}'_\perp)-\psi_{\nu-+}^{\pm\dagger}(x,\mathbf{p}''_\perp)\psi_{\nu-+}^{\pm}(x,\mathbf{p}'_\perp)\\&+\psi_{\nu+0}^{\pm\dagger}(x,\mathbf{p}''_\perp)\psi_{\nu+0}^{\pm}(x,\mathbf{p}'_\perp)-\psi_{\nu-0}^{\pm\dagger}(x,\mathbf{p}''_\perp)\psi_{\nu-0}^{\pm}(x,\mathbf{p}'_\perp)\\&+\psi_{\nu+-}^{\pm\dagger}(x,\mathbf{p}''_\perp)\psi_{\nu+-}^{\pm}(x,\mathbf{p}'_\perp)-\psi_{\nu--}^{\pm\dagger}(x,\mathbf{p}''_\perp)\psi_{\nu--}^{\pm}(x,\mathbf{p}'_\perp)],\end{aligned} \tag{53}$$

$$\begin{aligned}W_A^{\nu[i\sigma^{j+}\gamma^5]}(\boldsymbol{\Delta}_\perp,\mathbf{p}_\perp,x;\pm\hat{S}_z)=\frac{1}{16\pi^3}\epsilon_\perp^{ij}[&(-i)^i\psi_{\nu++}^{\pm\dagger}(x,\mathbf{p}''_\perp)\psi_{\nu-+}^{\pm}(x,\mathbf{p}'_\perp)+(i)^i\psi_{\nu-+}^{\pm\dagger}(x,\mathbf{p}''_\perp)\psi_{\nu++}^{\pm}(x,\mathbf{p}'_\perp)\\&+(-i)^i\psi_{\nu+0}^{\pm\dagger}(x,\mathbf{p}''_\perp)\psi_{\nu-0}^{\pm}(x,\mathbf{p}'_\perp)+(i)^i\psi_{\nu-0}^{\pm\dagger}(x,\mathbf{p}''_\perp)\psi_{\nu+0}^{\pm}(x,\mathbf{p}'_\perp)\\&+(-i)^i\psi_{\nu+-}^{\pm\dagger}(x,\mathbf{p}''_\perp)\psi_{\nu--}^{\pm}(x,\mathbf{p}'_\perp)+(i)^i\psi_{\nu--}^{\pm\dagger}(x,\mathbf{p}''_\perp)\psi_{\nu+-}^{\pm}(x,\mathbf{p}'_\perp)],\end{aligned} \tag{54}$$

with the Dirac structures $\Gamma=\gamma^+,\gamma^+\gamma^5$ and $i\sigma^{j+}\gamma^5$, and where the initial and final momenta of the struck quark are

$$\mathbf{p}'_\perp=\mathbf{p}_\perp-(1-x)\frac{\boldsymbol{\Delta}_\perp}{2},\qquad \mathbf{p}''_\perp=\mathbf{p}_\perp+(1-x)\frac{\boldsymbol{\Delta}_\perp}{2}, \tag{55}$$

respectively. Using the light-front wave functions from Eqs. (3), (5), and (6) in Eqs. (49)–(54) at the initial scale μ_0, we explicitly calculate all the quark-quark correlators, which give the expressions of Wigner distributions in the following forms:

$$\rho_{UU}^{\nu(S)}=N_S^2\rho_1^\nu(\mathbf{b}_\perp,\mathbf{p}_\perp,x),\qquad \rho_{UU}^{\nu(A)}=\left(\frac{1}{3}N_0^{(\nu)2}+\frac{2}{3}N_1^{(\nu)2}\right)\rho_1^\nu(\mathbf{b}_\perp,\mathbf{p}_\perp,x), \tag{56}$$

$$\rho_{UL}^{\nu(S)}=-N_S^2\rho_2^\nu(\mathbf{b}_\perp,\mathbf{p}_\perp,x),\qquad \rho_{UL}^{\nu(A)}=-\left(\frac{1}{3}N_0^{(\nu)2}+\frac{2}{3}N_1^{(\nu)2}\right)\rho_2^\nu(\mathbf{b}_\perp,\mathbf{p}_\perp,x), \tag{57}$$

$$\rho_{UT}^{\nu j(S)}=N_S^2\rho_3^{\nu j}(\mathbf{b}_\perp,\mathbf{p}_\perp,x),\qquad \rho_{UT}^{\nu j(A)}=\left(\frac{1}{3}N_0^{(\nu)2}+\frac{2}{3}N_1^{(\nu)2}\right)\rho_3^{\nu j}(\mathbf{b}_\perp,\mathbf{p}_\perp,x), \tag{58}$$

$$\rho_{LU}^{\nu(S)}=N_S^2\rho_2^\nu(\mathbf{b}_\perp,\mathbf{p}_\perp,x),\qquad \rho_{LU}^{\nu(A)}=\left(\frac{1}{3}N_0^{(\nu)2}-\frac{2}{3}N_1^{(\nu)2}\right)\rho_2^\nu(\mathbf{b}_\perp,\mathbf{p}_\perp,x), \tag{59}$$

$$\rho_{LL}^{\nu(S)} = N_S^2 \rho_4^\nu(\mathbf{b}_\perp, \mathbf{p}_\perp, x), \qquad \rho_{LL}^{\nu(A)} = \left(\frac{1}{3}N_0^{(\nu)2} - \frac{2}{3}N_1^{(\nu)2}\right)\rho_4^\nu(\mathbf{b}_\perp, \mathbf{p}_\perp, x), \tag{60}$$

$$\rho_{LT}^{\nu j(S)} = -N_S^2 \rho_5^{\nu j}(\mathbf{b}_\perp, \mathbf{p}_\perp, x), \qquad \rho_{LT}^{\nu j(A)} = -\left(\frac{1}{3}N_0^{(\nu)2} - \frac{2}{3}N_1^{(\nu)2}\right)\rho_5^{\nu j}(\mathbf{b}_\perp, \mathbf{p}_\perp, x), \tag{61}$$

$$\rho_{TU}^{i\nu(S)} = N_S^2 \rho_3^{i\nu}(\mathbf{b}_\perp, \mathbf{p}_\perp, x), \qquad \rho_{TU}^{i\nu(A)} = \frac{1}{3}N_0^{(\nu)2}\rho_3^{i\nu}(\mathbf{b}_\perp, \mathbf{p}_\perp, x), \tag{62}$$

$$\rho_{TL}^{i\nu(S)} = N_S^2 \rho_5^{i\nu}(\mathbf{b}_\perp, \mathbf{p}_\perp, x), \qquad \rho_{TU}^{i\nu(A)} = -\frac{1}{3}N_0^{(\nu)2}\rho_5^{i\nu}(\mathbf{b}_\perp, \mathbf{p}_\perp, x), \tag{63}$$

$$\rho_{TT}^{\nu(S)} = N_S^2 \rho_6^{\nu}(\mathbf{b}_\perp, \mathbf{p}_\perp, x), \qquad \rho_{TT}^{\nu(A)} = -\frac{1}{3}N_0^{(\nu)2}\rho_6^{\nu}(\mathbf{b}_\perp, \mathbf{p}_\perp, x), \tag{64}$$

$$\rho_{TT}^{\perp qS} = -N_S^2 \rho_7^{\nu}(\mathbf{b}_\perp, \mathbf{p}_\perp, x), \qquad \rho_{TT}^{\perp qA} = \frac{1}{3}N_0^{(\nu)2}\rho_7^{\nu}(\mathbf{b}_\perp, \mathbf{p}_\perp, x), \tag{65}$$

where the label S represents the scalar and A denotes the isoscalar-vector (V) diquark corresponding to the u quark and the isovector-vector (VV) diquark corresponding to the d quark. Combining the contributions from the scalar and vector parts, one can write the distributions for u and d as

$$\rho_{NN'}^{u}(\mathbf{b}_\perp, \mathbf{p}_\perp, x) = C_S^2 \rho_{NN'}^{u(S)} + C_V^2 \rho_{NN'}^{u(A)}, \tag{66}$$

$$\rho_{NN'}^{d}(\mathbf{b}_\perp, \mathbf{p}_\perp, x) = C_{VV}^2 \rho_{NN'}^{d(A)}, \tag{67}$$

where $N(N')$ implies the proton (quark) polarization. Now, integrating over the light-front momentum fraction x, we display the behavior of the Wigner distributions in the remaining four dimensions; i.e. in the transverse coordinate space with a definite transverse momentum and in the transverse momentum space with a definite coordinate.

The distribution functions $\rho_i^\nu(\mathbf{b}_\perp, \mathbf{p}_\perp, x)$ are given by

$$\rho_1^\nu(\mathbf{b}_\perp, \mathbf{p}_\perp, x) = \frac{1}{16\pi^3}\int \frac{d\Delta_\perp}{2\pi}\Delta_\perp \mathrm{J}_0(|\Delta_\perp||b_\perp|)\exp(-2\tilde{\mathrm{a}}(\mathrm{x})\tilde{\mathbf{p}}_\perp^2)\left[|A_1^\nu(x)|^2 + \left(\mathbf{p}_\perp^2 - \frac{\mathbf{\Delta}_\perp^2}{4}(1-x)^2\right)\frac{1}{M^2x^2}|A_2^\nu(x)|^2\right], \tag{68}$$

$$\rho_2^\nu(\mathbf{b}_\perp, \mathbf{p}_\perp, x) = \frac{1}{M^2}\epsilon_\perp^{ij}p_\perp^i\frac{\partial}{\partial b_\perp^j}\left[\frac{1}{16\pi^3}\int \frac{d\Delta_\perp}{2\pi}\Delta_\perp \mathrm{J}_0(|\Delta_\perp||b_\perp|)\exp(-2\tilde{\mathrm{a}}(\mathrm{x})\tilde{\mathbf{p}}_\perp^2)\frac{(1-x)}{x^2}|A_2^\nu(x)|^2\right], \tag{69}$$

$$\rho_3^{\nu j}(\mathbf{b}_\perp, \mathbf{p}_\perp, x) = \epsilon_\perp^{ij}\frac{\partial}{\partial b_\perp^i}\frac{1}{16\pi^3}\int \frac{d\Delta_\perp}{2\pi}\Delta_\perp \mathrm{J}_0(|\Delta_\perp||b_\perp|)\exp(-2\tilde{\mathrm{a}}(\mathrm{x})\tilde{\mathbf{p}}_\perp^2)\frac{(1-x)}{xM}A_1^\nu(x)A_2^\nu(x), \tag{70}$$

$$\rho_4^\nu(\mathbf{b}_\perp, \mathbf{p}_\perp, x) = \frac{1}{16\pi^3}\int \frac{d\Delta_\perp}{2\pi}\Delta_\perp \mathrm{J}_0(|\Delta_\perp||b_\perp|)\exp(-2\tilde{\mathrm{a}}(\mathrm{x})\tilde{\mathbf{p}}_\perp^2)[|A_1^\nu(x)|^2 - (\mathbf{p}_\perp^2 - \frac{\mathbf{\Delta}_\perp^2}{4}(1-x)^2)\frac{1}{M^2x^2}|A_2^\nu(x)|^2], \tag{71}$$

$$\rho_5^{\nu j}(\mathbf{b}_\perp, \mathbf{p}_\perp, x) = \frac{1}{16\pi^3}\int \frac{d\Delta_\perp}{2\pi}\Delta_\perp \mathrm{J}_0(|\Delta_\perp||b_\perp|)\frac{2p^j}{xM}A_1^\nu(\mathrm{x})A_2^\nu(\mathrm{x})\exp(-2\tilde{\mathrm{a}}(\mathrm{x})\tilde{\mathbf{p}}_\perp^2), \tag{72}$$

$$\begin{aligned}\rho_6^\nu(\mathbf{b}_\perp, \mathbf{p}_\perp, x) = \frac{1}{16\pi^3}\int \frac{d^2\Delta_\perp}{(2\pi)^2}e^{-i\Delta_\perp\cdot\mathbf{b}_\perp}\Bigg[&|A_1^\nu(x)|^2 + \left(\mathbf{p}_\perp^2 - \frac{\mathbf{\Delta}_\perp^2}{4}(1-x)^2\right)\frac{1}{x^2M^2}|A_2^\nu(x)|^2 \\ &- \delta_{ij}\left(p^ip^j - \frac{\Delta^i\Delta^j}{4}(1-x)^2\right)\frac{2}{x^2M^2}|A_2^\nu(x)|^2\Bigg]\exp(-2\tilde{a}(x)\tilde{\mathbf{p}}_\perp^2),\end{aligned} \tag{73}$$

$$\rho_7^\nu(\mathbf{b}_\perp, \mathbf{p}_\perp, x) = \frac{1}{16\pi^3}\int \frac{d^2\Delta_\perp}{(2\pi)^2}e^{-i\Delta_\perp\cdot\mathbf{b}_\perp}\epsilon_\perp^{ij}\left(p^ip^j - \frac{\Delta^i\Delta^j}{4}(1-x)^2\right)\frac{2}{x^2M^2}|A_2^\nu(x)|^2\exp(-2\tilde{a}(x)\tilde{\mathbf{p}}_\perp^2), \tag{74}$$

with

$$A_i^\nu(x) = \frac{4\pi}{\kappa}\sqrt{\frac{\log(1/x)}{(1-x)}}x^{a_i^\nu}(1-x)^{b_i^\nu}, \tag{75}$$

$$\tilde{a}(x) = \frac{\log(1/x)}{2\kappa^2(1-x)^2}, \tag{76}$$

$$\tilde{\mathbf{p}}_\perp^2 = \mathbf{p}_\perp^2 + \frac{\mathbf{\Delta}_\perp^2}{4}(1-x)^2. \tag{77}$$

Note that there is no implicit sum over i and j in the expression of ρ_6^ν and ρ_7^ν.

A. Unpolarized proton

We plot the first Mellin moment of the unpolarized Wigner distribution, $\rho_{UU}^\nu(\mathbf{b}_\perp, \mathbf{p}_\perp, x)$, and mixing distributions, $\tilde{\rho}_{UU}^\nu(b_x, p_y, x)$ for the u and d quarks in Fig. 1. The first Mellin moment of the unpolarized Wigner distributions represents the transverse phase-space distribution of the unpolarized quark in an unpolarized proton. Figs. 1(a) and 1(d) show the distributions in the transverse momentum plane for the u quark and d quark, respectively, with a fixed impact parameter $\mathbf{b}_\perp$ along $\hat{y}$ and $b_y = 0.4$ fm, whereas the variation of the distributions in the transverse impact parameter plane are shown in Figs. 1(b) and 1(e), with a fixed transverse momentum $\mathbf{p}_\perp$ along $\hat{y}$ for $p_y = 0.3$ GeV. Figures 1(c) and 1(f) represent the mixing distributions for the u quark and d quark, respectively.

The average quadrupole distortions $Q_b^{ij}(\mathbf{p}_\perp)$ and $Q_p^{ij}(\mathbf{b}_\perp)$ are defined as [8]

$$Q_b^{ij}(\mathbf{p}_\perp) = \frac{\int d^2\mathbf{b}_\perp(2b_\perp^i b_\perp^j - \delta^{ij}\mathbf{b}_\perp^2)\rho_{UU}(\mathbf{b}_\perp, \mathbf{p}_\perp)}{\int d^2\mathbf{b}_\perp \mathbf{b}_\perp^2 \rho_{UU}(\mathbf{b}_\perp, \mathbf{p}_\perp)}, \tag{78}$$

$$Q_p^{ij}(\mathbf{b}_\perp) = \frac{\int d^2\mathbf{p}_\perp(2p_\perp^i p_\perp^j - \delta^{ij}\mathbf{p}_\perp^2)\rho_{UU}(\mathbf{b}_\perp, \mathbf{p}_\perp)}{\int d^2\mathbf{p}_\perp \mathbf{p}_\perp^2 \rho_{UU}(\mathbf{b}_\perp, \mathbf{p}_\perp)}. \tag{79}$$

Since the wave functions in the soft-wall AdS/QCD model are of Gaussian type, the average quadrupole distortion is found to be zero for ρ_{UU}^ν. Similarly, ρ_{LL}^ν has zero quadrupole distortion. Therefore, the distributions ρ_{UU}^ν in the transverse momentum plane as well as the transverse impact parameter plane are circularly symmetric, but the distributions in mixed space are axially symmetric. Thus, there is no favored configuration between $\mathbf{b}_\perp \perp \mathbf{p}_\perp$ and $\mathbf{b}_\perp \| \mathbf{p}_\perp$ in mixed space, unlike with the light-cone constituent quark model (LCCQM) [7] or the chiral quark soliton model (χQSM) [8]. Comparing the behaviors of the u quark and the d quark, one finds in this model that for both u and d quarks, the distributions have positive maxima at the center $(p_x = p_y = 0)$, $(b_x = b_y = 0)$ in both planes, and they gradually decrease towards periphery. The peaks of the distributions for the u quark are large compared to those for the d quark, but the u-quark distributions have little concentration in the center relative to the d-quark distributions in both planes. The distributions have similar spread behaviors in the mixed plane for u and d quarks.

In Fig. 2, we plot the unpolarized longitudinal Wigner distribution, which represents the transverse phase-space distribution of the longitudinally polarized quark in an unpolarized proton. The transverse Wigner distributions $\rho_{UL}^\nu(\mathbf{b}_\perp, \mathbf{p}_\perp)$ in the transverse momentum plane with a fixed impact parameter $\mathbf{b}_\perp$ along $\hat{y}$ are presented in Figs. 2(a) and 2(d) for u and d quarks, respectively. Figures 2(b) and 2(e) show the same distributions in the transverse impact parameter plane for u and d quarks with fixed $\mathbf{p}_\perp = p_y\hat{y} = 0.3$ GeV. We find in this model that in both planes ρ_{UL}^ν exhibits dipolar structures having the same polarity for u and d quarks, but the polarity in momentum space is opposite from that for coordinate space for each quark. ρ_{UL}^ν in the transverse momentum plane is more concentrated in the center than in the transverse coordinate plane. The mixing distribution $\tilde{\rho}_{UL}^\nu(b_x, p_y)$ in the transverse mixed plane is shown in Figs. 2(c) and 2(f) for u and d quarks, respectively, displaying the quadrupole structures with the same polarity for both quarks. These distributions essentially reflect quark spin-orbit correlations. From Eq. (47), we calculate C_z^ν at $\mu^2 = 1$ GeV^2, and the values are $C_z^u = -0.55$ and $C_z^d = -0.75$ for u and d quarks, respectively. $C_z^\nu < 0$ implies that the quark OAM is antiparallel to the quark spin, as observed in the scalar diquark model [17], whereas in the light-cone constituent quark model [8], the C_z^ν values are found to be positive for both u and d quarks.

The Wigner distribution $\rho_{UT}(\mathbf{b}_\perp, \mathbf{p}_\perp)$ and the mixing distribution $\bar{\rho}_{UT}(b_y, p_x)$ are shown in Fig. 3. From Eq. (58), it is clear that this distribution vanishes if the quark transverse coordinate is parallel to the polarization. Here the plots are shown for $j = 1$, and the quark is polarized along the x direction. Figures 3(a) and 3(d) represent the distributions in the transverse momentum plane for u and d quarks, respectively, with $\mathbf{b}_\perp = 0.4\hat{y}$ fm. This is circularly symmetric in transverse momentum space. Figures 3(b) and 3(e) show the distributions in the transverse impact parameter plane for u and d quarks, respectively, with $\mathbf{p}_\perp = 0.3\hat{x}$ GeV. We see a dipolar distribution in the impact parameter plane. The mixing distribution $\bar{\rho}_{UT}(b_y, p_x)$ is shown in Figs. 3(c) and 3(f) for u and d quarks, respectively. Since this distribution is symmetric in the transverse momentum plane, it shows a dipolar behavior in the mixed plane [unlike $\bar{\rho}_{UL}(b_x, p_y)$, which shows a quadrupole distribution]. Because of the dipolar symmetry in the impact parameter plane, the other class of mixing distributions, $\tilde{\rho}_{UT}(b_x, p_y)$, vanishes.

In a certain kinematical limit [see Eq. (31)], $\rho_{UT}(\mathbf{b}_\perp, \mathbf{p}_\perp, x)$ reduces to the Boer-Mulders function

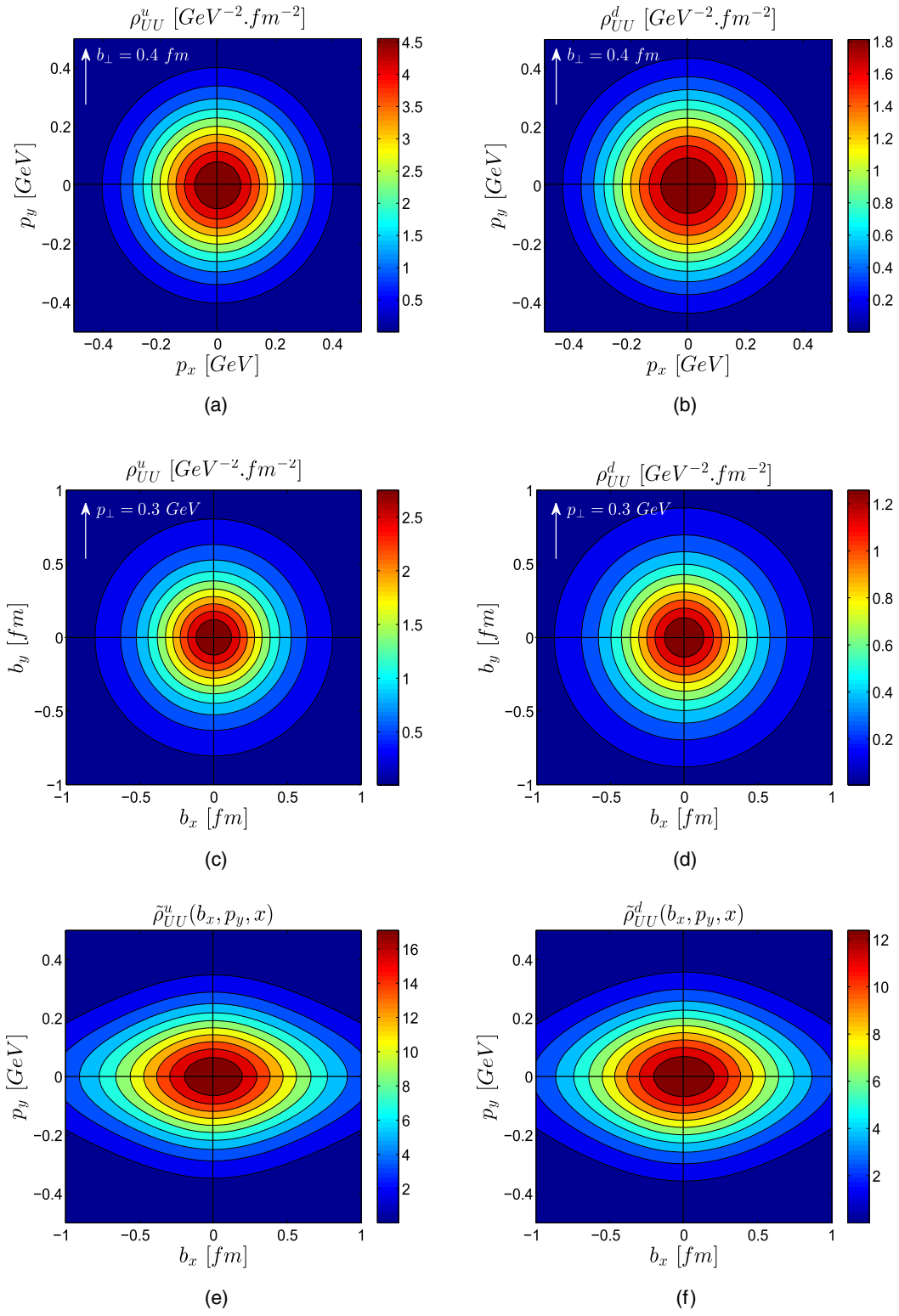

FIG. 1. The distributions ρ_{UU} are shown in the transverse momentum plane, the transverse coordinate plane, and the mixed plane for u and d quarks. The distributions in the mixed plane are given in $\mathrm{GeV}^0\,\mathrm{fm}^0$.

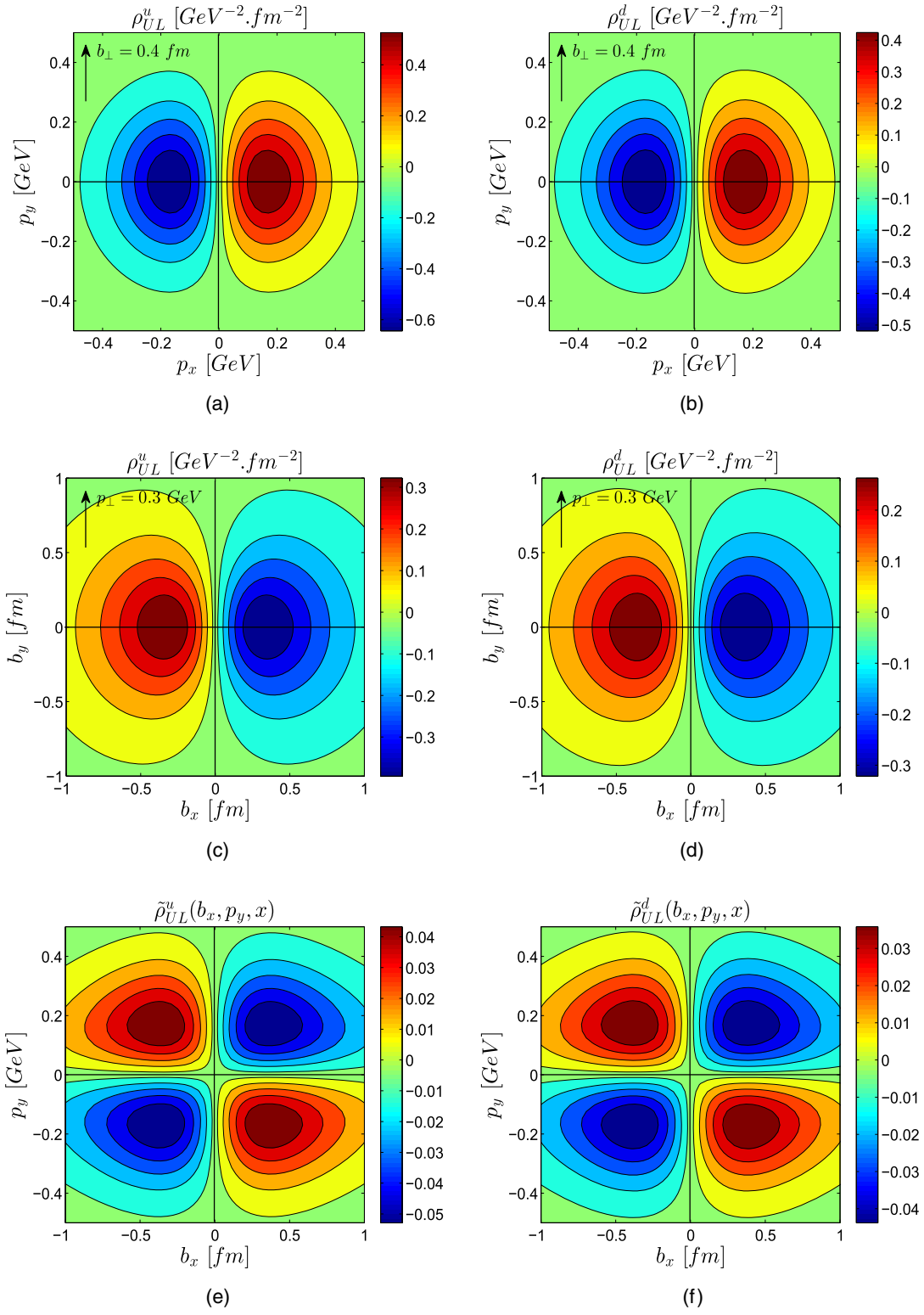

FIG. 2. The distributions ρ_{UL} are presented in the transverse momentum plane, the transverse coordinate plane, and the mixed plane for u and d quarks. The distributions in the mixed plane are given in $\mathrm{GeV}^0\,\mathrm{fm}^0$.

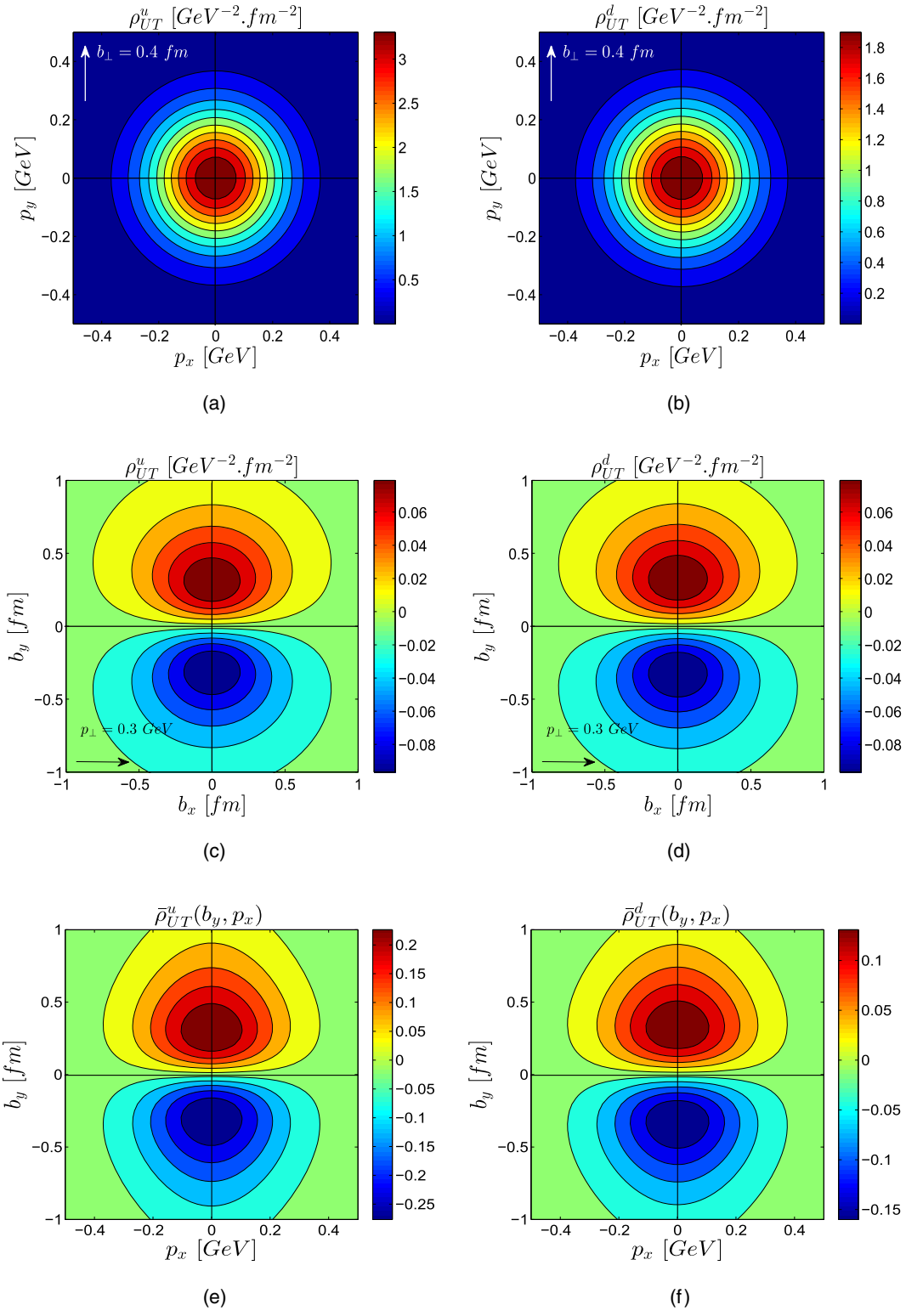

FIG. 3. The distribution ρ_{UT} is shown in the transverse momentum plane [(a) and (d)] with $\mathbf{b}_\perp = 0.4\hat{y}$ fm, in the transverse coordinate plane [(b) and (e)] with $\mathbf{p}_\perp = 0.3\hat{x}$ GeV, and in the mixed plane [(c) and (f)] for u and d quarks. The distributions in the mixed planes are given in $\mathrm{GeV}^0\,\mathrm{fm}^0$. The quark is transversely polarized along the x-axis.

$h_1^{\perp}(x, \mathbf{p}_\perp)$, which is one of the T-odd TMDs at leading twist. Here we consider the T-even leading-twist TMDs only. The one-gluon final-state interaction (FSI) is needed to calculate the T-odd TMDs. So, here we have no contribution from this distribution at the TMD limit. At the impact parameter distribution limit, the distribution is related to $\tilde{H}_T$ GPD together with some other distributions [4].

B. Longitudinally polarized proton

In Fig. 4, we show the longitudinal unpolarized Wigner distributions $\rho^{\nu}_{LU}(\mathbf{b}_\perp, \mathbf{p}_\perp)$ and mixing distributions $\tilde{\rho}^{\nu}_{LU}(b_x, p_y)$ which describe the unpolarized quark phase-space distributions in a longitudinal polarized proton. Figures 4(a) and 4(d) display the variation of $\rho^{\nu}_{LU}(\mathbf{b}_\perp, \mathbf{p}_\perp)$ in the transverse momentum plane for u and d quarks, respectively, with fixed $\mathbf{b}_\perp$ along $\hat{y}$ and $b_y = 0.4$ fm; and the variation of $\rho^{\nu}_{LU}(\mathbf{b}_\perp, \mathbf{p}_\perp)$ in the transverse impact parameter plane is shown in Figs. 4(b) and 4(e) with fixed $\mathbf{p}_\perp$ along $\hat{y}$, $p_y = 0.3$ GeV. In this model, the distributions $\rho^{\nu}_{LU}(\mathbf{b}_\perp, \mathbf{p}_\perp)$ are quite similar to $\rho^{\nu}_{UL}(\mathbf{b}_\perp, \mathbf{p}_\perp)$ in both transverse momentum and transverse impact parameter planes, but the polarity of the dipolar structures of ρ^{ν}_{LU} is opposite to the polarity of ρ^{ν}_{UL}. Again, the quadrupole structures appear when we plot the distribution in the transverse mixed plane, as shown in Figs. 4(c) and 4(f) for u and d quarks, respectively, which are very similar to $\tilde{\rho}^{\nu}_{UL}(b_x, p_y)$ with opposite sign. These distributions essentially reflect the correlations between quark OAM and proton spin. In this model, the quark OAM $\ell^u_z = 0.49$ for the u quark and $\ell^d_z = 0.58$ for the d quark at $\mu^2 = 1$ GeV^2. Therefore, the quark OAM is parallel to the proton spin for both u and d quarks. Note also that in a scalar diquark model with AdS/QCD wave functions, the OAMs are found to be positive for both quarks. This result is model dependent and may be due to the particular form of the AdS/QCD wave functions.

The longitudinal-longitudinal Wigner distributions $\rho^{\nu}_{LL}(\mathbf{b}_\perp, \mathbf{p}_\perp)$ and mixing distributions $\tilde{\rho}^{\nu}_{LL}(b_x, p_y)$ are presented in Fig. 5. These Wigner distributions describe the phase-space distributions of longitudinal polarized quarks in a longitudinal polarized proton, and after integrating over transverse variables they correspond to the axial charge (Δq), which is positive for the u quark but negative for the d quark at large scales. The distributions $\rho^{\nu}_{LL}(\mathbf{b}_\perp, \mathbf{p}_\perp)$ in the transverse momentum plane for u and d quarks are plotted in Figs. 5(a) and 5(d), respectively, whereas $\rho^{\nu}_{LL}(\mathbf{b}_\perp, \mathbf{p}_\perp)$ in the transverse coordinate plane are shown in Figs. 5(b) and 5(e). In this model, we find that in two planes the distributions are positive for the u quark in consistence with the sign of Δu; but for the d quark, the distributions are also positive, whereas the axial charge Δd is known to be negative. One should note that the axial charges are highly scale dependent and are measured only at high energies, whereas the models here have a very low initial scale of $\mu_0 = 0.313$ GeV. So, we need to consider the scale evolution of the distributions before comparing with the measured data. For the d quark, the axial charge is known to be negative at larger scales. The scale evolutions of axial charges in this model are shown in Ref. [18], where it is shown that the axial charge for the d quark becomes negative for $\mu^2 \geq 0.15$ GeV^2. At $\mu^2 = 1$ GeV^2, the axial charges for the quarks are found to be $g^u_A = 0.73$ and $g^d_A = -0.54$, which are values consistent with the measured data. The distributions are circularly symmetric for u and d quarks in both the planes, and they are more concentrated in the center in the $\mathbf{b}_\perp$ plane relative to the $\mathbf{p}_\perp$ plane. The peaks of the distributions in the $\mathbf{p}_\perp$ plane are larger than those in the $\mathbf{b}_\perp$ plane. The mixing distributions $\tilde{\rho}^{\nu}_{LL}(b_x, p_y)$ for u and d quarks are shown in Figs. 5(c) and 5(f), respectively. They are axially symmetric in the mixed plane. $\tilde{\rho}^{\nu}_{LL}(b_x, p_y)$ show quite similar behavior to $\tilde{\rho}^{\nu}_{UU}(b_x, p_y)$, but with opposite sign and with a much lower peak at the center.

The Wigner distribution with a transversely polarized quark in a longitudinally polarized proton, $\rho_{LT}(\mathbf{b}_\perp, \mathbf{p}_\perp)$, is shown in Fig. 6. Figures 6(a) and 6(d) represent the distribution in the transverse momentum plane, with $\mathbf{b}_\perp = 0.4\hat{y}$ fm, for u and d quarks, respectively. We see a dipolar distribution, as expected from Eq. (61). Figures 6(b) and 6(e) show the distribution in transverse coordinate space, with $\mathbf{p}_\perp = 0.3\hat{x}$ GeV, for u and d quarks, respectively. The distribution is circularly symmetric with a negative peak at the center of the coordinate space. The distribution vanishes if the quark transverse momentum is perpendicular to the polarization. This reflects that there is a strong correlation between the quark transverse momentum and quark transverse polarization. The mixing distribution $\bar{\rho}_{LT}(b_y, p_x)$ is shown in Figs. 6(c) and 6(f) for u and d quarks, respectively. Because of the dipolar structure in the transverse momentum plane, the other class of mixing distributions $\tilde{\rho}_{LT}(b_x, p_y)$ vanishes for the quark with a polarization along the x-axis.

At the TMD limit, $\rho_{LT}(\mathbf{b}_\perp, \mathbf{p}_\perp, x)$ reduces to $h^{\perp}_{1L}(x, \mathbf{p}_\perp)$ [4], one of the eight T-even TMDs at leading twist. At the impact parameter distribution limit, the distribution is related to the H_T and $\tilde{H}_T$ GPD together with some other distributions.

C. Transversely polarized proton

The Wigner distribution $\rho_{TU}(\mathbf{b}_\perp, \mathbf{p}_\perp)$ in transverse planes and the mixing distribution $\bar{\rho}_{TU}(b_y, p_x)$ are shown in Fig. 7. From Eq. (62), it is clear that this distribution vanishes if the quark transverse coordinate is parallel to the polarization. Here the plots are shown for $j = 1$; i.e. the quark is polarized along the x direction. Figures 3(a) and 3(d) represent the distribution in the transverse momentum plane, with $\mathbf{b}_\perp = 0.4\hat{y}$ fm, for u and d quarks, respectively. This is circularly symmetric in transverse

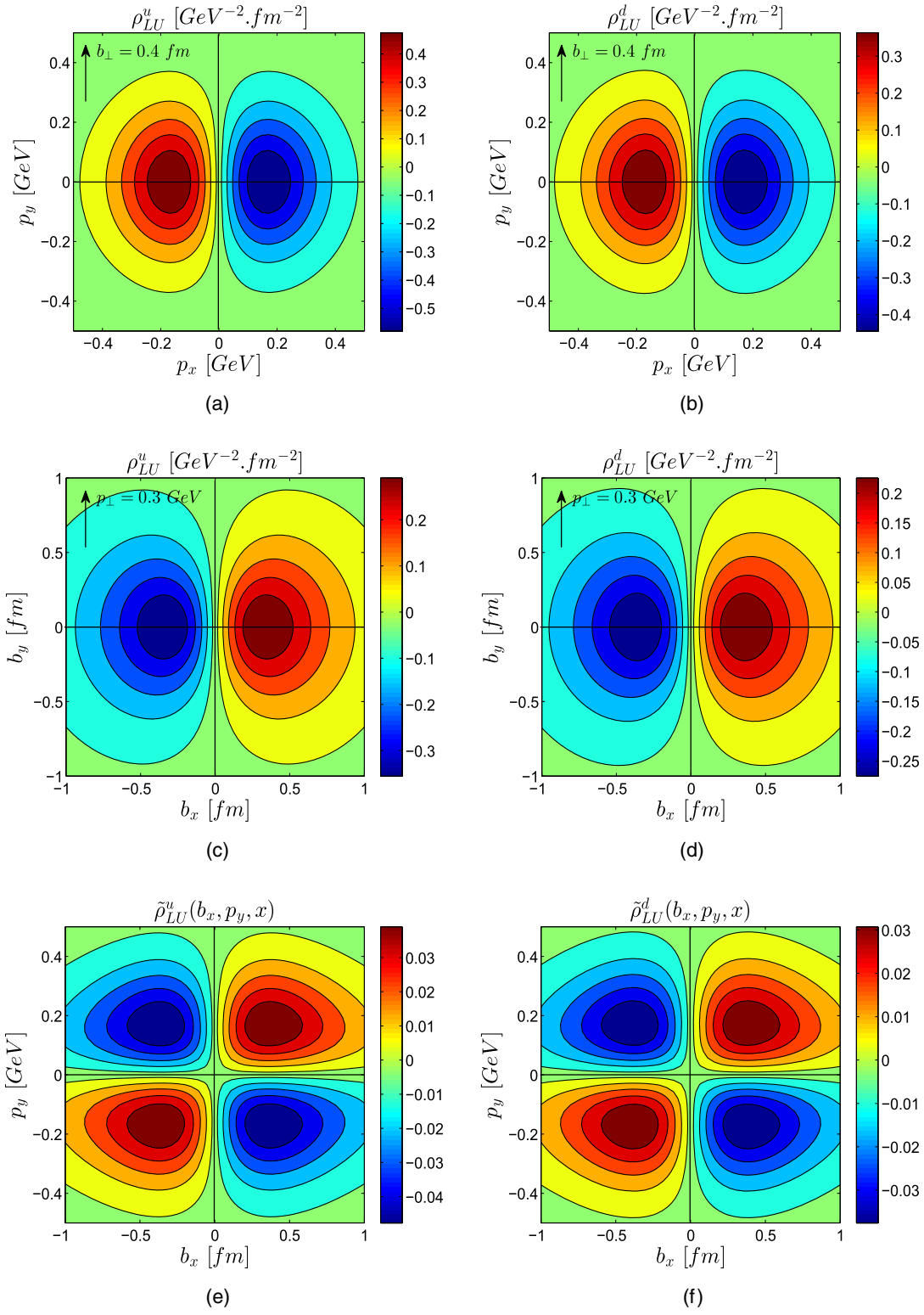

FIG. 4. The distributions ρ_{LU} are shown in the transverse momentum plane, in the transverse coordinate plane, and in the mixed plane for u and d quarks. The distributions in the mixed plane are given in $\mathrm{GeV}^0\,\mathrm{fm}^0$.

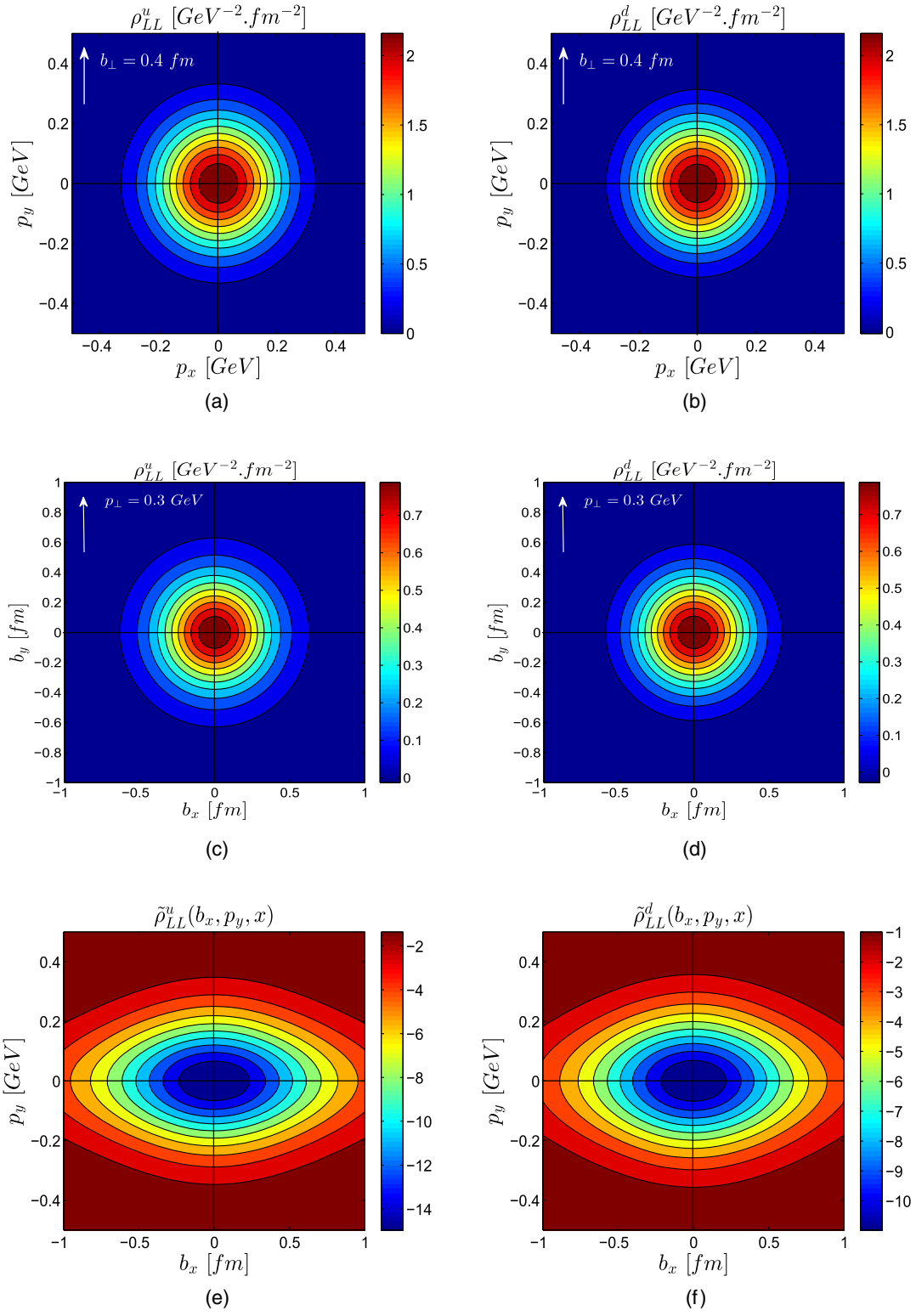

FIG. 5. The distributions ρ_{LL} are shown in the transverse momentum plane, in the transverse coordinate plane, and in the mixed plane for u and d quarks. The distributions in the mixed plane are given in $\mathrm{GeV}^0\,\mathrm{fm}^0$.

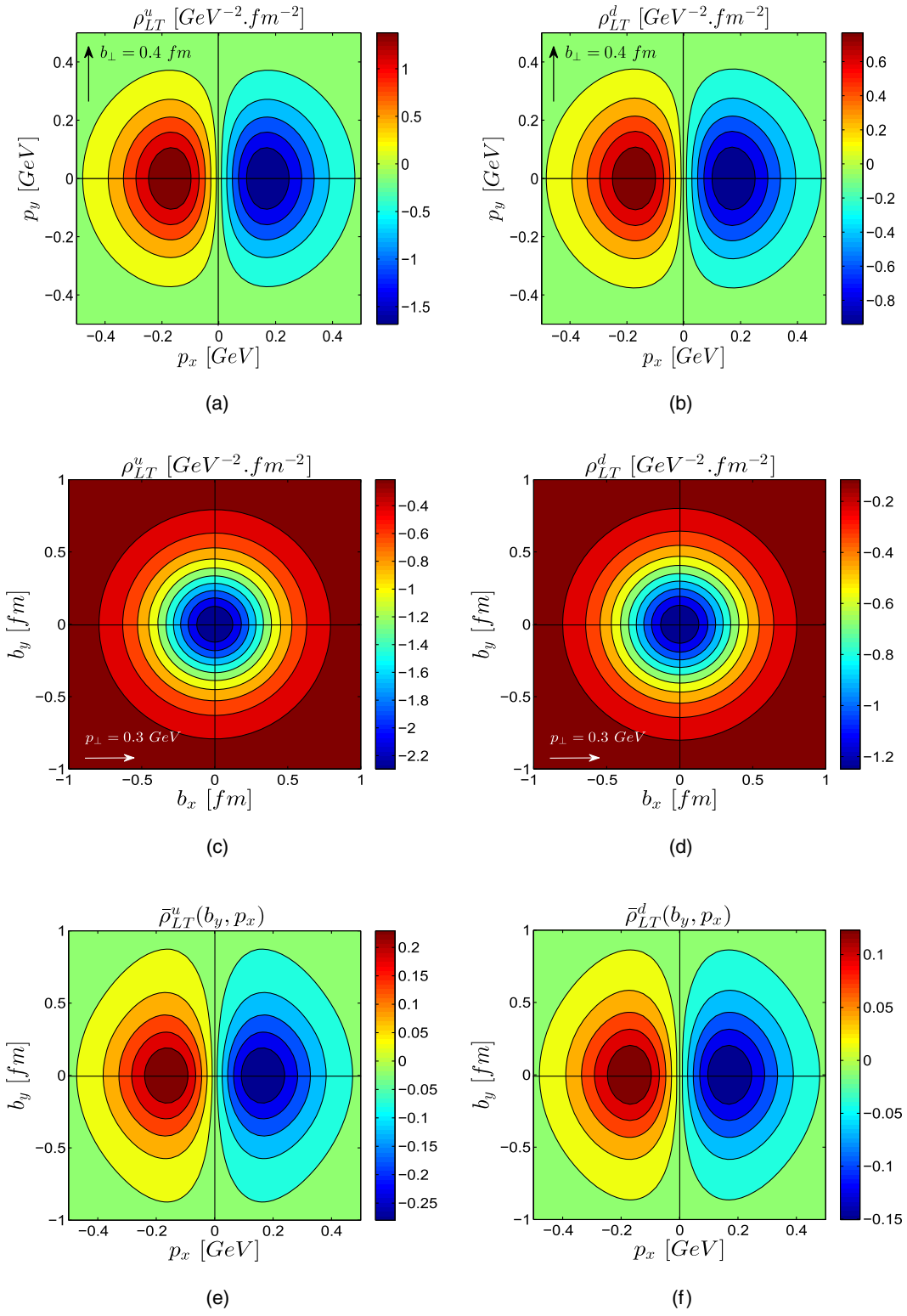

FIG. 6. The distributions ρ_{LT} are shown in the transverse momentum plane [(a) and (d)] with $\mathbf{b}_\perp = 0.4\hat{y}$ fm, in the transverse coordinate plane [(b) and (e)] with $\mathbf{p}_\perp = 0.3\hat{x}$ GeV, and in the mixed plane [(c) and (f)] for u and d quarks. The quark is polarized along the x-axis. The distributions in the mixed planes are given in $\mathrm{GeV}^0\ \mathrm{fm}^0$.

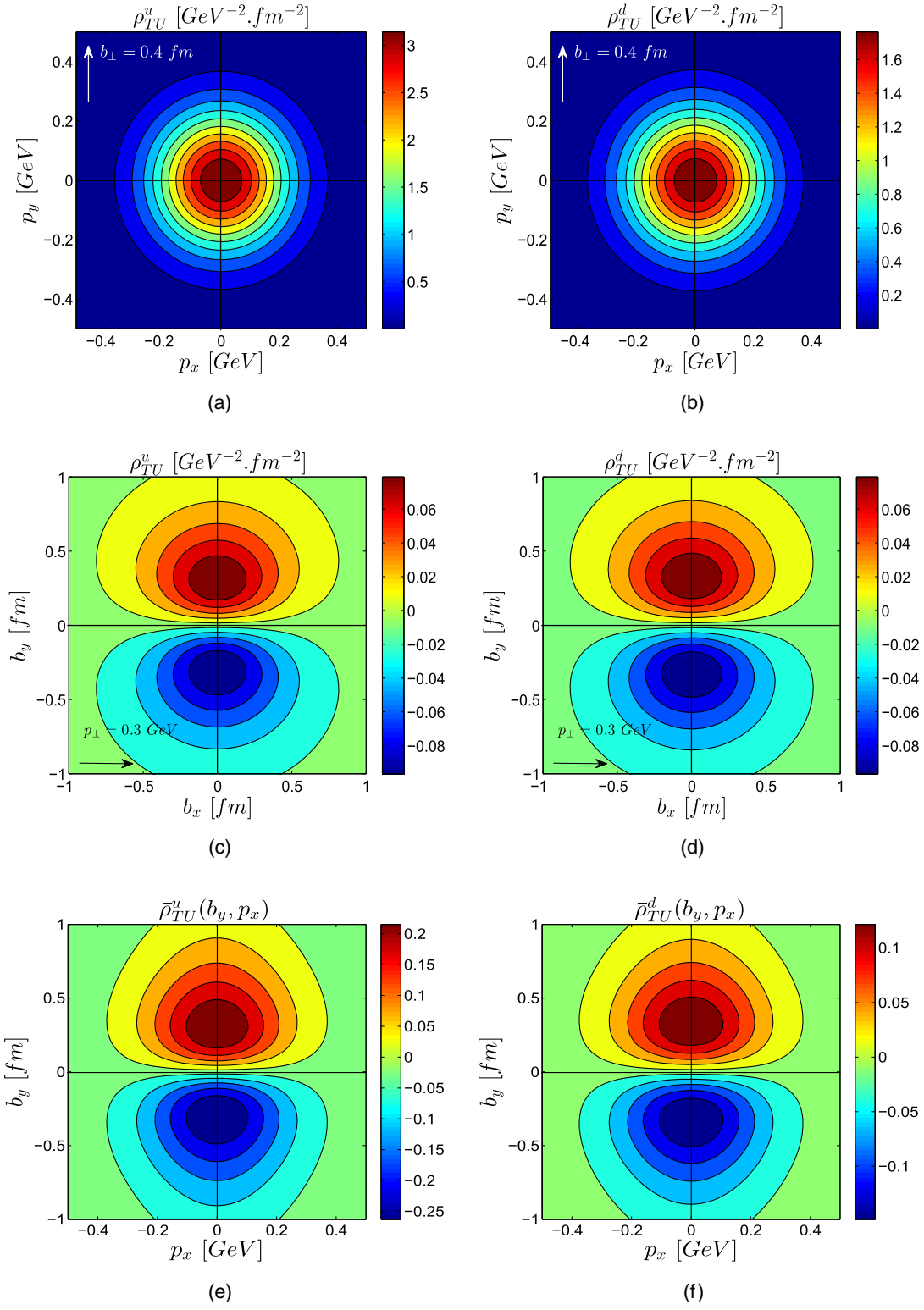

FIG. 7. The distributions $\rho_{TU}(\mathbf{b}_\perp, \mathbf{p}_\perp)$ are presented in the transverse momentum plane [(a) and (d)] with $\mathbf{b}_\perp = 0.4\hat{y}$ fm, in the transverse coordinate plane [(b) and (e)] with $\mathbf{p}_\perp = 0.3\hat{x}$ GeV, and in the mixed plane [(c) and (f)] for u and d quarks. The distributions in the mixed planes are given in $\mathrm{GeV}^0\,\mathrm{fm}^0$.

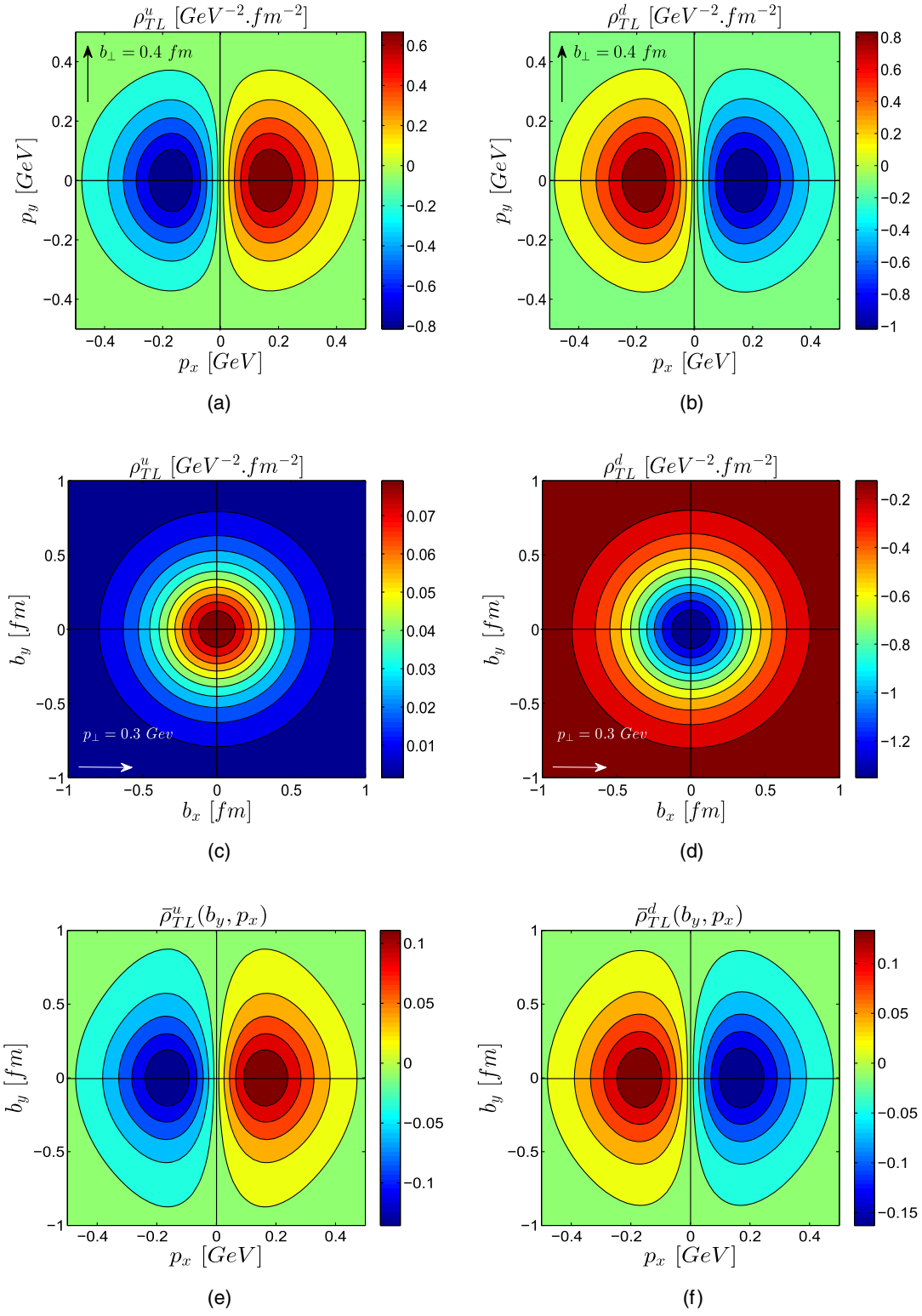

FIG. 8. The distributions $\rho_{TL}(\mathbf{b}_\perp, \mathbf{p}_\perp)$ are shown in the transverse momentum plane [(a) and (d)] with $\mathbf{b}_\perp = 0.4\hat{y}$ fm, in the transverse coordinate plane [(b) and (e)] with $\mathbf{p}_\perp = 0.3\hat{x}$ GeV, and in the mixed plane [(c) and (f)] for u and d quarks. The polarization of the proton is taken along the x-axis. The distributions in the mixed planes are given in $\mathrm{GeV}^0\ \mathrm{fm}^0$.

momentum space. Figures 7(b) and 7(e) show the distribution in transverse coordinate space, with $\mathbf{p}_\perp = 0.3\hat{y}$ GeV, for u and d quarks, respectively. We see a dipolar distribution in the impact parameter plane. The mixing distribution $\bar{\rho}_{TU}(b_y, p_x)$ is shown in Figs. 7(c) and 7(f) for u and d quarks, respectively. Since this distribution is symmetric in the transverse momentum plane, it shows a dipolar behavior in the mixed plane [unlike $\bar{\rho}_{UL}(b_x, p_y)$, which shows a quadruple distribution]. Because of the dipolar structure in coordinate space, the other class of mixing distributions $\tilde{\rho}_{TU}(b_x, p_y)$ vanishes.

At the TMD limit, $\rho_{TU}(\mathbf{b}_\perp, \mathbf{p}_\perp, x)$ reduces to the Sivers function $f_{1T}^{\perp}(x, \mathbf{p}_\perp)$, one of the T-odd TMDs at leading twist. Since we consider T-even contributions only, the TMD limit of $\rho_{TU}(\mathbf{b}_\perp, \mathbf{p}_\perp)$ vanishes here. At the impact parameter distribution limit, the distribution is related to the H and E GPDs together with some other distributions.

The Wigner distribution with a longitudinally polarized quark in a transversely polarized proton, $\rho_{TL}(\mathbf{b}_\perp, \mathbf{p}_\perp)$, is shown in Fig. 8. Figures 8(a) and 8(d) represent the distribution in the transverse momentum plane, with $\mathbf{b}_\perp = 0.4\hat{y}$ fm, for u and d quarks, respectively. We see a dipolar distribution as expected from Eq. (63). Figures 6(b) and 6(e) show the distribution in transverse coordinate space, with $\mathbf{p}_\perp = 0.3\hat{x}$ GeV, for u and d quarks, respectively. The distribution is circularly symmetric at the center of the coordinate space with a positive peak for the u quark and a negative peak for the d quark.

The distribution vanishes if the quark transverse momentum is perpendicular to the polarization. This reflects that there is a strong correlation between the quark transverse momentum and quark transverse polarization. The mixing distribution $\bar{\rho}_{TL}(b_y, p_x)$ is shown in Figs. 8(c) and 8(f) for u and d quarks, respectively. Because of the dipolar structure in the transverse momentum plane, the other class of mixing distributions $\tilde{\rho}_{TL}(b_x, p_y)$ vanishes for the quark with a polarization along the x-axis.

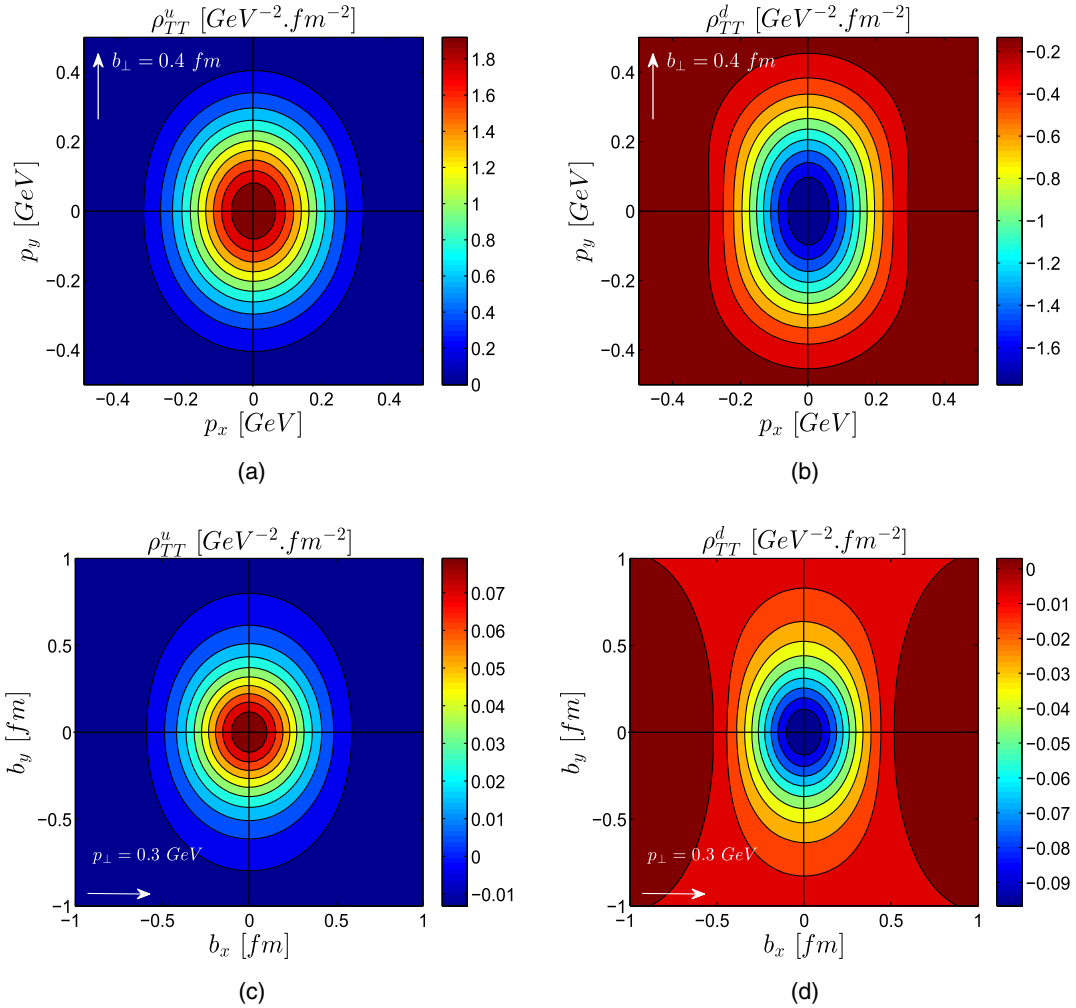

FIG. 9. The distributions $\rho_{TT}(\mathbf{b}_\perp, \mathbf{p}_\perp)$ are shown in the transverse momentum plane [(a) and (c)] with $\mathbf{b}_\perp = 0.4\hat{y}$ fm and in the transverse coordinate plane [(b) and (d)] with $\mathbf{p}_\perp = 0.3\hat{x}$ GeV for u and d quarks. The proton polarization and the quark polarization are taken along the x-axis.

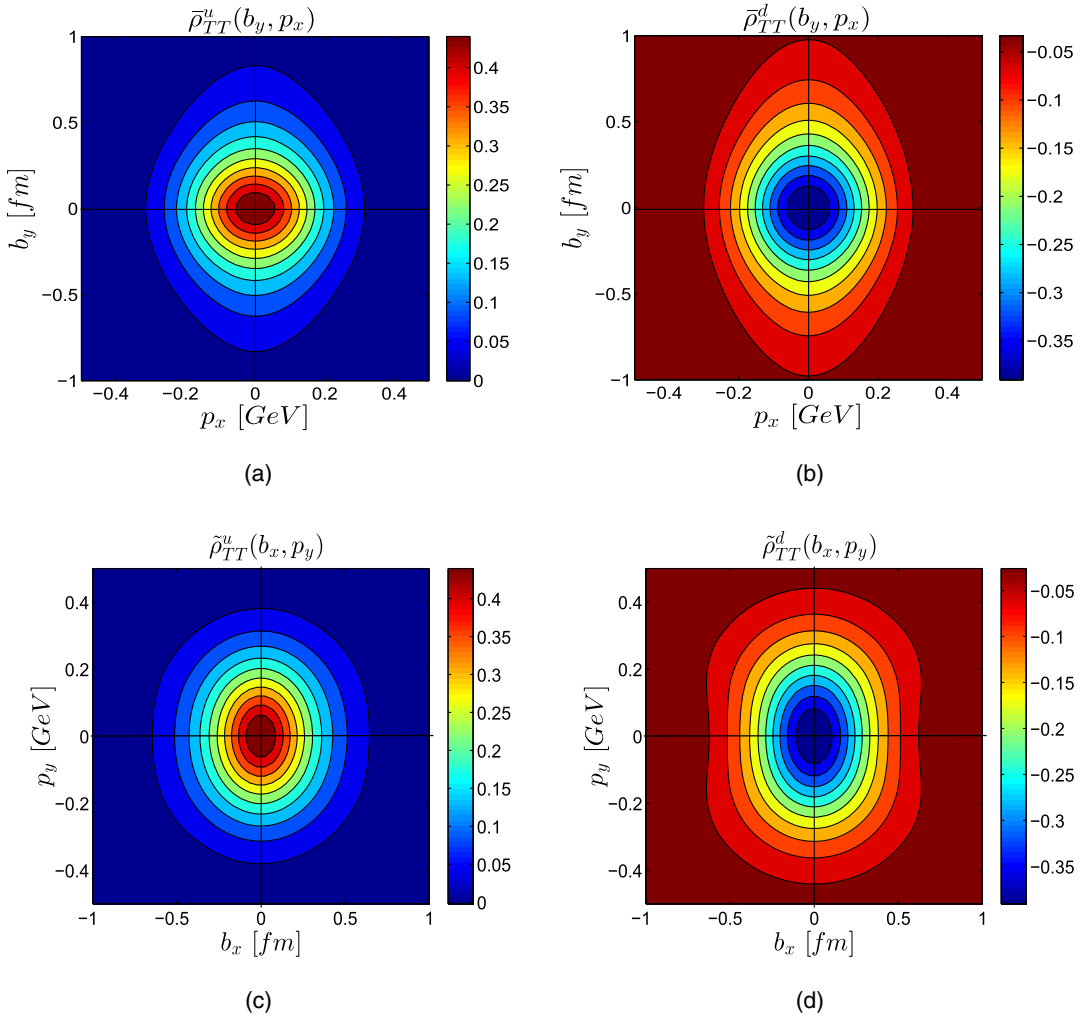

FIG. 10. The distributions $\tilde{\rho}_{TT}(by, px)$ and $\tilde{\rho}_{TT}(bx, py)$ are shown in the transverse mixed planes for u and d quarks. The quark and proton both are polarized along the x-axis. The distributions are given in $\mathrm{GeV}^0\ \mathrm{fm}^0$.

At the TMD limit, $\rho_{TL}(\mathbf{b}_\perp, \mathbf{p}_\perp)$ reduces to $g_{1T}(x, \mathbf{p}_\perp)$ [4], one of the eight T-even TMDs at leading twist. At the impact parameter distribution limit, the distribution is related to $\tilde{H}$ and $\tilde{E}$ GPDs together with some other distributions.

The Wigner distribution with a transversely polarized quark in a transversely polarized proton, $\rho_{TT}(\mathbf{b}_\perp, \mathbf{p}_\perp)$, is shown in Fig. 9. Figures 9(a) and 9(c) represent the distribution in the transverse momentum plane, with $\mathbf{b}_\perp = 0.4\hat{y}$ fm, for u and d quarks, respectively. The distribution in the transverse impact parameter plane is shown in Figs. 9(b) and 9(d), with $\mathbf{p}_\perp = 0.3\hat{x}$ GeV. We observe that the peaks of the distribution in both the planes are positive for the u quark and negative for the d quark. In Fig. 10, we plot $\rho_{TT}(\mathbf{b}_\perp, \mathbf{p}_\perp)$ in the mixed transverse plane for u and d quarks. The distributions are not symmetric in the mixed plane. This is due to the quadrupole contributions $p^i p^j$ and $\Delta^i \Delta^j$ appearing in the expressions for ρ^ν_6 [Eq. (73)].

The pretzelous distribution, $\rho^\perp_{TT}(\mathbf{b}_\perp, \mathbf{p}_\perp)$, is shown in Fig. 11. This distribution is found when the quark is transversely polarized along the perpendicular direction to the transversely polarized proton. We find quadruple distributions in the transverse momentum plane as well as in the transverse impact parameter plane. It is also observed that the polarity of quadruple distribution changes sign for the d quark in both the planes. Due to the pure quadrupole contribution in ρ^ν_7 [Eq. (74)], the pretzelous distribution is identically zero in the mixed plane.

D. Spin-spin correlations

The longitudinal Wigner distributions $\rho^\nu_{\Lambda\lambda}(\mathbf{b}_\perp, \mathbf{p}_\perp)$, with proton polarization $\Lambda = \uparrow$ and quark polarization $\lambda = \uparrow, \downarrow$ [Eq. (24)], are shown in Figs. 12 and 13 for the u and d quarks, respectively. One can observe that the distributions $\rho^\nu_{\Lambda\lambda}(\mathbf{b}_\perp, \mathbf{p}_\perp)$ in the transverse momentum plane as well as in the transverse impact parameter plane look circularly symmetric for $\Lambda = \lambda$, whereas for $\Lambda \neq \lambda$ the distributions

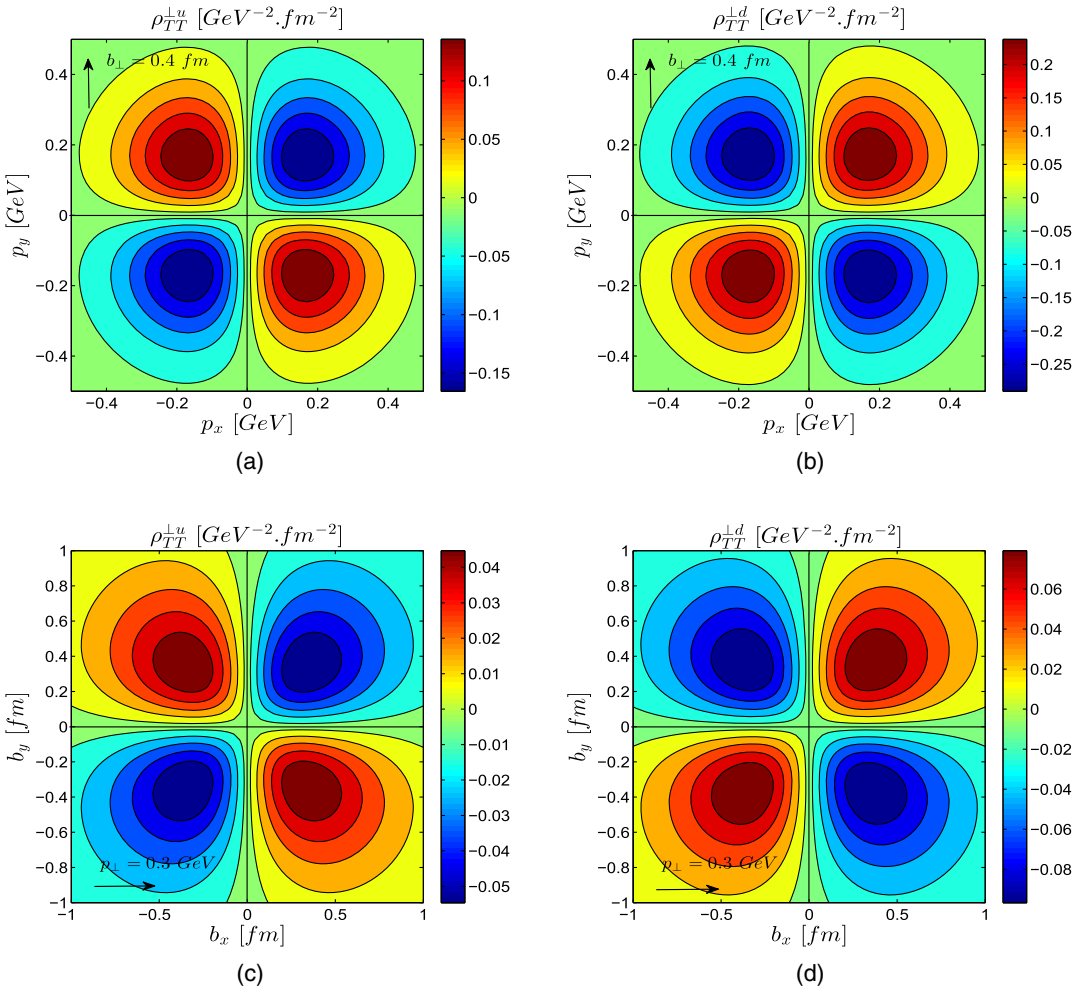

FIG. 11. The distributions $\rho_{TT}^{\perp}(\mathbf{b}_\perp, \mathbf{p}_\perp)$ are shown in the transverse momentum plane and in the transverse coordinate plane for u and d quarks. The quark is polarized along the y-axis, and the proton is polarized along the x-axis.

get distorted along p_x or b_x for both u and d quarks. Since the polarity of ρ_{UL}^{ν} is opposite to that of ρ_{LU}^{ν} and the magnitudes of the distributions are more or less the same, in Eq. (24), the contributions from ρ_{LU} and ρ_{UL} are almost canceled for $\Lambda = \lambda$, and the only dominating contributions come from ρ_{UU} and ρ_{LL}, which are circularly symmetric in both planes. Again, for $\Lambda \neq \lambda$ the contributions from ρ_{LU} and ρ_{UL} add up and cause the distortion. Note that the distortions from the circular symmetry in the transverse momentum plane and in the transverse impact parameter plane are in opposite directions to each other. Here we have shown the distributions for $\Lambda = \uparrow$; the other possible spin combinations in the transverse momentum plane and in the transverse impact parameter plane can be found from $\rho_{\downarrow\lambda'}^{\nu}(\mathbf{b}_\perp, p_x, p_y) = \rho_{\uparrow\lambda}^{\nu}(\mathbf{b}_\perp, -p_x, p_y)$ and $\rho_{\downarrow\lambda'}^{\nu}(b_x, b_y, \mathbf{p}_\perp) = \rho_{\uparrow\lambda}^{\nu}(-b_x, b_y, \mathbf{p}_\perp)$, respectively, where $\lambda' \neq \lambda$. The mixed transverse densities $\tilde{\rho}_{\Lambda\lambda}^{\nu}(b_x, p_y)$ are shown in Figs. 12(c) and 12(f) for the u quark, and in Figs. 13(c) and 13(f) for the d quark. $\tilde{\rho}_{\Lambda\lambda}^{\nu}(b_x, p_y)$ exhibits the similar axially symmetric nature of $\tilde{\rho}_{UU}(b_x, p_y)$ with a lower magnitude for $\Lambda = \lambda$. This is because of the other contribution, $\tilde{\rho}_{LL}(b_x, p_y)$, which is opposite to that of $\tilde{\rho}_{UU}(b_x, p_y)$. For $\Lambda \neq \lambda$, although there are additional quadrupole contributions from $\tilde{\rho}_{UL}$ and $\tilde{\rho}_{LU}$ in $\tilde{\rho}_{\uparrow\downarrow}(b_x, p_y)$, the contributions from ρ_{UU} and ρ_{LL} are very large compared to the quadrupole contributions, and thus $\tilde{\rho}_{\uparrow\downarrow}(b_x, p_y)$ effectively show the similar behavior of $\tilde{\rho}_{UU}$ with larger magnitude for both u and d quarks.

We observe that the quark OAM tends to be aligned with the proton spin and antialigned with the quark spin for both u and d quarks. The difference in correlation strength between the quark OAM–proton spin correlation and the quark OAM–spin correlation is very small (see Figs. 2 and 4). Therefore, if the quark spin is parallel to the proton spin, i.e. $\Lambda = \uparrow, \lambda = \uparrow$, the contributions of ρ_{UL} and ρ_{LU} interfere destructively, resulting in circular symmetry for the u and d quarks; see Figs. 12(a), 12(b), 13(a), and 13(b). If the quark spin is antiparallel to the

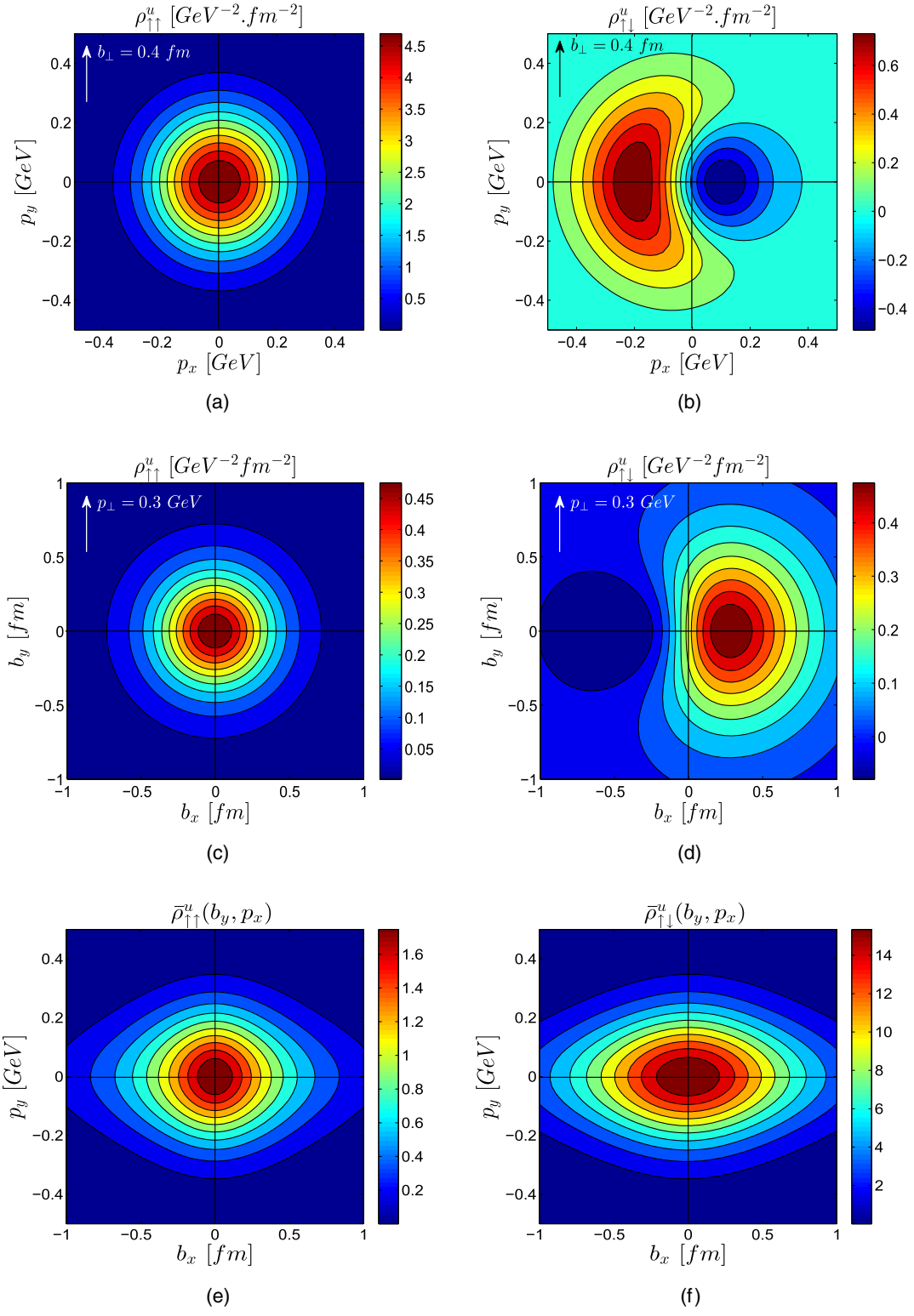

FIG. 12. The distributions $\rho_{\Lambda\lambda}$ are shown in the transverse momentum plane, the transverse impact parameter plane and the mixed plane for the u quark [Eq. (24)]. The distributions in the mixed plane are given in $\mathrm{GeV}^0\ \mathrm{fm}^0$.

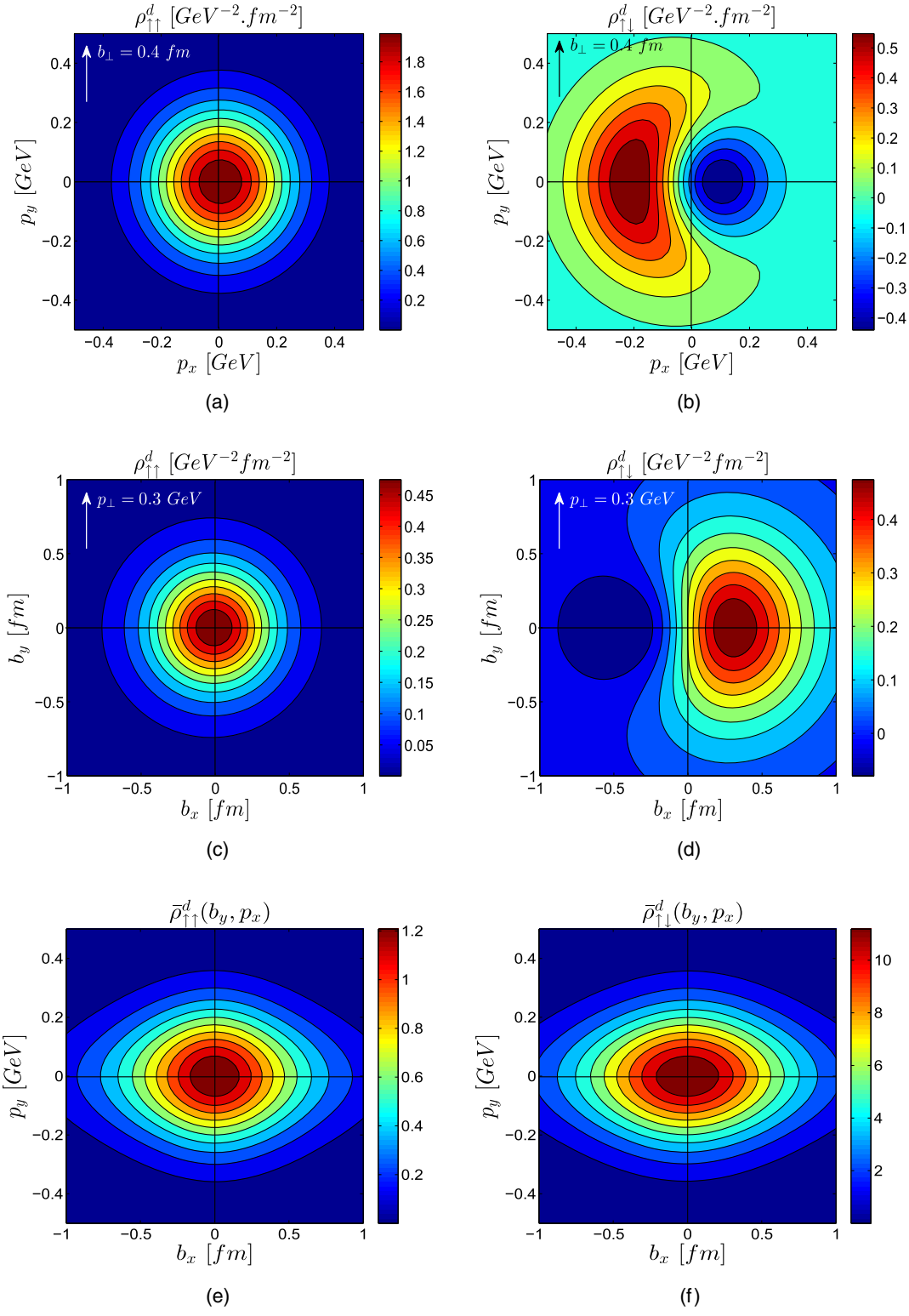

FIG. 13. The distributions $\rho_{\Lambda\lambda}$ are shown in the transverse momentum plane, the transverse coordinate plane and the mixed plane for d quarks. The distributions in the mixed plane are given in $\mathrm{GeV}^0\,\mathrm{fm}^0$.

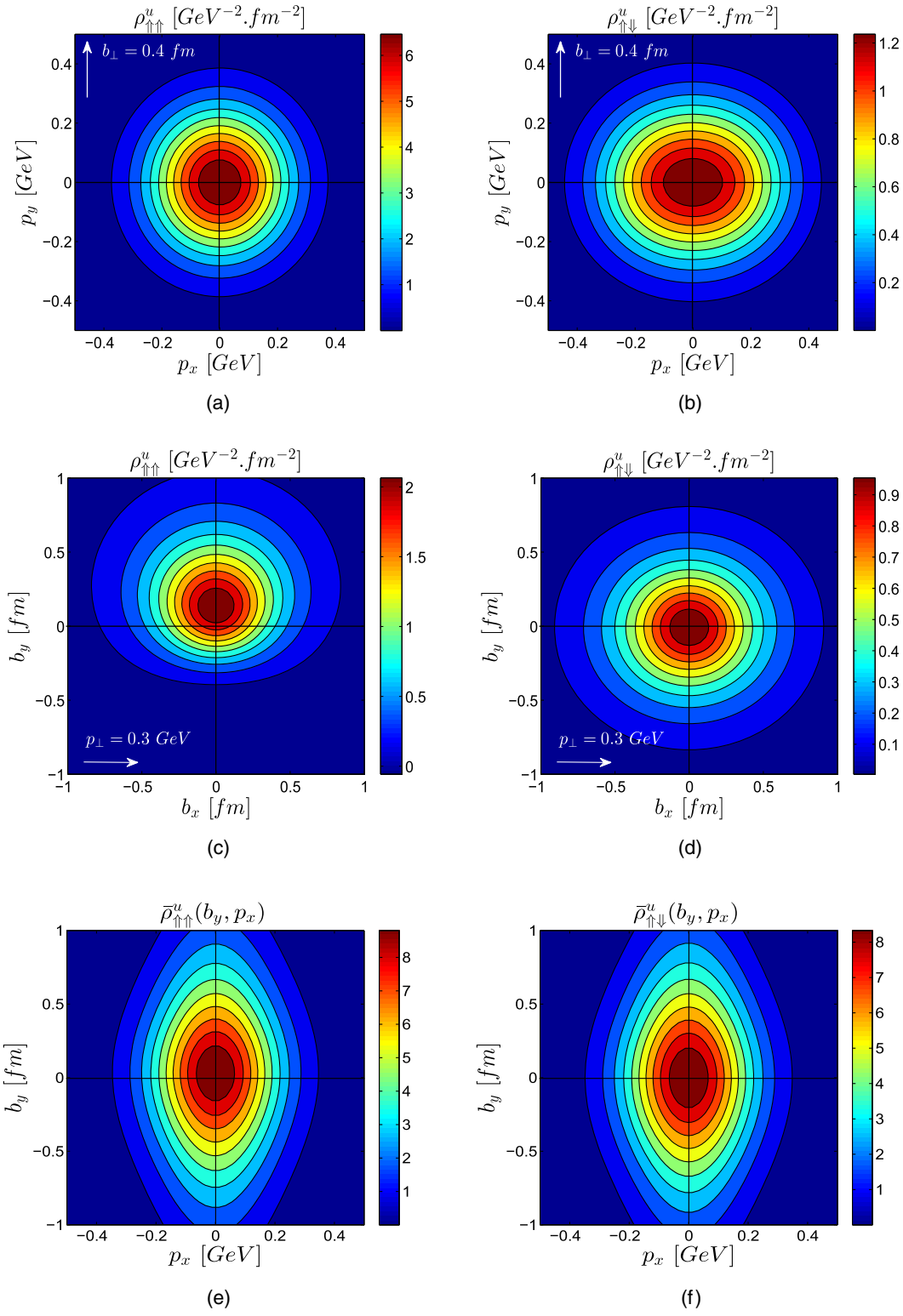

FIG. 14. $\rho_{\Lambda_T\lambda_T}$ in the transverse momentum plane, the transverse impact parameter plane and the mixed plane for the u quark [Eq. (26)]. $\Lambda_T = \Uparrow, \Downarrow$ and $\lambda_T = \Uparrow, \Downarrow$ represent the transverse polarization along the x-axis for protons and quarks, respectively. The mixed plane distributions are given in $\mathrm{GeV}^0\,\mathrm{fm}^0$.

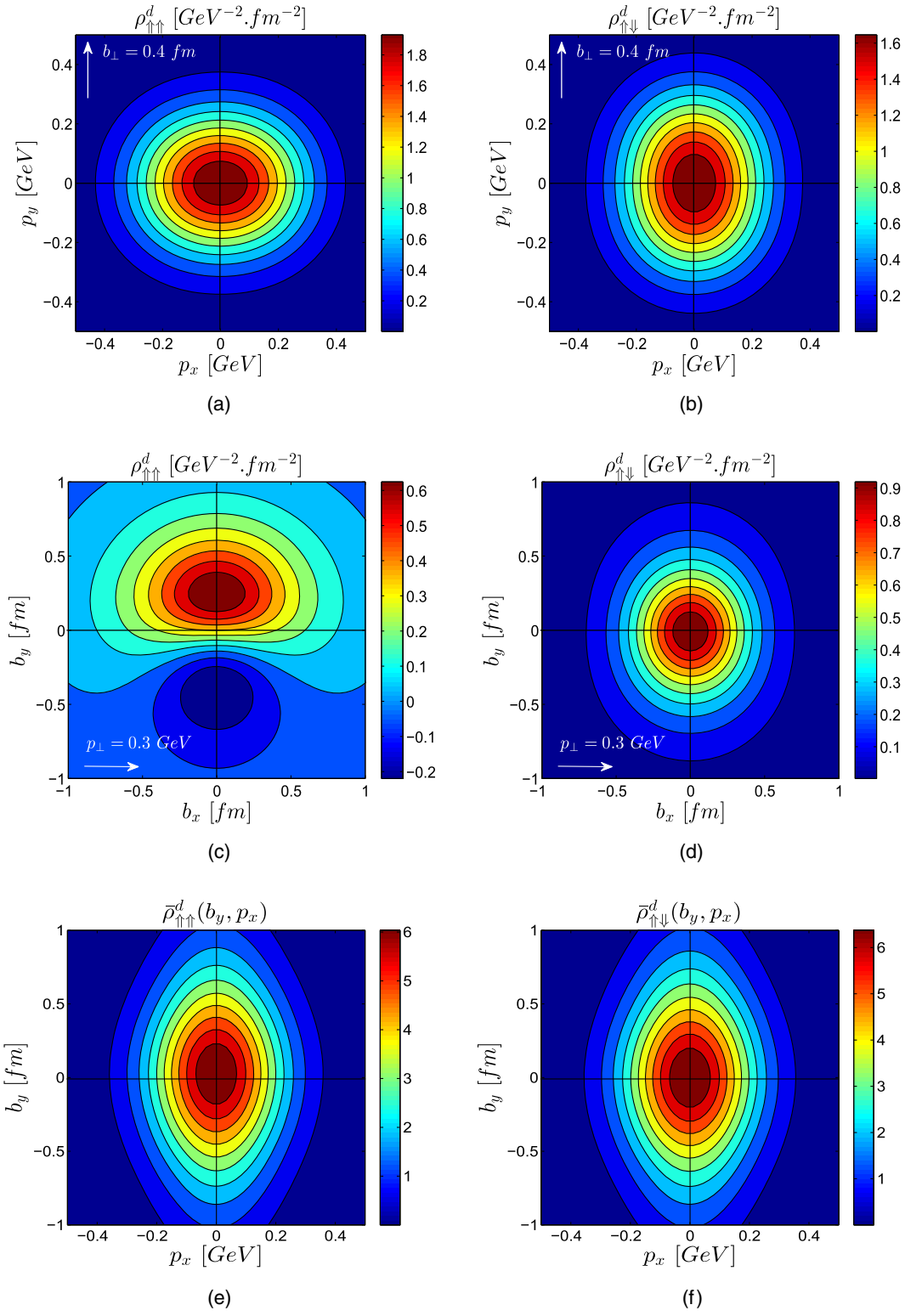

FIG. 15. $\rho_{\Lambda_T\lambda_T}$ in the transverse momentum plane, the transverse impact parameter plane and the mixed plane for the d quark [Eq. (26)]. $\Lambda_T = \Uparrow, \Downarrow$ and $\lambda_T = \Uparrow, \Downarrow$ represent the transverse polarization along the x-axis for proton and quarks, respectively. The distributions in the mixed plane are given in $\mathrm{GeV}^0\,\mathrm{fm}^0$.

proton spin, i.e. $\Lambda = \uparrow, \lambda = \downarrow$, the contributions of ρ_{UL} and ρ_{LU} interfere constructively, resulting in a dipolar distribution for the u and d quarks; see Figs. 12(d), 12(e), 13(d), and 13(e).

From Eq. (26), we plot the transverse Wigner distribution $\rho_{\Lambda_T\lambda_T}(\mathbf{b}_\perp, \mathbf{p}_\perp)$ in Fig. 14 for the u quark and in Fig. 15 for the d quark to understand the transverse spin-spin correlations. Figure 14 represents the distribution of a u quark with transverse polarization $\lambda_T = \Uparrow, \Downarrow$ (along the x-axis) in a proton with transverse polarization $\Lambda_T = \Uparrow$ along the x-axis. In the transverse momentum plane, we see an elliptical distribution for both the quarks [Figs. 14(a), 14(d), 15(a), and 15(d)] because the distortions ρ_{TU}, ρ_{UT} are circularly symmetric and ρ_{TT} is elliptically symmetric. In the transverse impact parameter plane, we observe that significant deviation comes from the dipolar nature of the distortions ρ^{ν}_{UT} and ρ^{ν}_{TU}. For $\Lambda_T\lambda_T = \Uparrow\Uparrow$, they interfere constructively and cause a large deviation, as seen in Figs. 14(b) and 15(b). We also observe that the distributions change axis with the flip of transverse polarization of quarks.

VI. GTMDS AND THEIR EVOLUTION

The generalized transverse-momentum-dependent distributions can be extracted from the different Wigner distributions as shown in Eqs. (29)–(38). The GTMDs reduce to the TMDs and GPDs at certain kinematical limits. $F_{1,4}$ and $G_{1,1}$ contribute to the spin-OAM correlation, as discussed in Sec. IV. $F_{1,4}$ and the OAM in the MIT bag model have been calculated in Ref. [27]. There are altogether 11 nonzero GTMDs at the leading twist in this model. In this model, comparing Eqs. (29)–(38) with Eq. (56)–(65), the explicit forms of the GTMDs are

$$F^{\nu}_{1,1}(x, \boldsymbol{\Delta}^2_\perp, \mathbf{p}^2_\perp) = N^{\nu}_{UU}\frac{1}{16\pi^3}\left[|A^{\nu}_1(x)|^2 + \left(\mathbf{p}^2_\perp - \frac{\boldsymbol{\Delta}^2_\perp}{4}(1-x)^2\right)\frac{1}{M^2x^2}|A^{\nu}_2(x)|^2\right]\exp[-2\tilde{a}(x)\tilde{\mathbf{p}}^2_\perp], \tag{80}$$

$$F^{\nu}_{1,2}(x, \boldsymbol{\Delta}^2_\perp, \mathbf{p}^2_\perp) = 0, \tag{81}$$

$$F^{\nu}_{1,3}(x, \boldsymbol{\Delta}^2_\perp, \mathbf{p}^2_\perp) = \frac{1}{2}F^{\nu}_{1,1}(x, \boldsymbol{\Delta}^2_\perp, \mathbf{p}^2_\perp) + N^{\nu}_{TU}\frac{1}{16\pi^3}\left[\frac{(1-x)}{x}A^{\nu}_1(x)A^{\nu}_2(x)\right]\exp[-2\tilde{a}(x)\tilde{\mathbf{p}}^2_\perp], \tag{82}$$

$$F^{\nu}_{1,4}(x, \boldsymbol{\Delta}^2_\perp, \mathbf{p}^2_\perp) = -N^{\nu}_{LU}\frac{1}{16\pi^3}\left[\frac{(1-x)}{x^2}|A^{\nu}_2(x)|^2\right]\exp[-2\tilde{a}(x)\tilde{\mathbf{p}}^2_\perp], \tag{83}$$

$$G^{\nu}_{1,1}(x, \boldsymbol{\Delta}^2_\perp, \mathbf{p}^2_\perp) = N^{\nu}_{UL}\frac{1}{16\pi^3}\left[\frac{(1-x)}{x^2}|A^{\nu}_2(x)|^2\right]\exp[-2\tilde{a}(x)\tilde{\mathbf{p}}^2_\perp], \tag{84}$$

$$G^{\nu}_{1,2}(x, \boldsymbol{\Delta}^2_\perp, \mathbf{p}^2_\perp) = N^{\nu}_{TL}\frac{1}{16\pi^3}\left[\frac{2}{x}A^{\nu}_1(x)A^{\nu}_2(x)\right]\exp[-2\tilde{a}(x)\tilde{\mathbf{p}}^2_\perp], \tag{85}$$

$$G^{\nu}_{1,3}(x, \boldsymbol{\Delta}^2_\perp, \mathbf{p}^2_\perp) = 0, \tag{86}$$

$$G^{\nu}_{1,4}(x, \boldsymbol{\Delta}^2_\perp, \mathbf{p}^2_\perp) = N^{\nu}_{LL}\frac{1}{16\pi^3}\left[|A^{\nu}_1(x)|^2 - \left(\mathbf{p}^2_\perp - \frac{\boldsymbol{\Delta}^2_\perp}{4}(1-x)^2\right)\frac{1}{M^2x^2}|A^{\nu}_2(x)|^2\right]\exp[-2\tilde{a}(x)\tilde{\mathbf{p}}^2_\perp], \tag{87}$$

$$H^{\nu}_{1,1}(x, \boldsymbol{\Delta}^2_\perp, \mathbf{p}^2_\perp) = 0, \tag{88}$$

$$H^{\nu}_{1,2}(x, \boldsymbol{\Delta}^2_\perp, \mathbf{p}^2_\perp) = N^{\nu}_{UT}\frac{1}{16\pi^3}\left[\frac{(1-x)}{x}A^{\nu}_1(x)A^{\nu}_2(x)\right]\exp[-2\tilde{a}(x)\tilde{\mathbf{p}}^2_\perp] \tag{89}$$

$$\begin{aligned} H^{\nu}_{1,3}(x, \boldsymbol{\Delta}^2_\perp, \mathbf{p}^2_\perp) = {} & N^{\nu}_{TT}\frac{1}{16\pi^3}\left[|A^{\nu}_1(x)|^2 + \left(\mathbf{p}^2_\perp - \frac{\boldsymbol{\Delta}^2_\perp}{4}(1-x)^2\right)\frac{1}{M^2x^2}|A^{\nu}_2(x)|^2\right] \\ & \times \exp[-2\tilde{a}(x)\tilde{\mathbf{p}}^2_\perp] - \frac{1}{2M^2}\Delta^2_\perp H^{\nu}_{1,2}(x, \boldsymbol{\Delta}^2_\perp, \mathbf{p}^2_\perp), \end{aligned} \tag{90}$$

$$H^{\nu}_{1,4}(x, \boldsymbol{\Delta}^2_\perp, \mathbf{p}^2_\perp) = N^{\perp\nu}_{TT}\frac{1}{16\pi^3}\left[\frac{2}{x^2}|A^{\nu}_2|^2\right]\exp[-2\tilde{a}(x)\tilde{\mathbf{p}}^2_\perp], \tag{91}$$

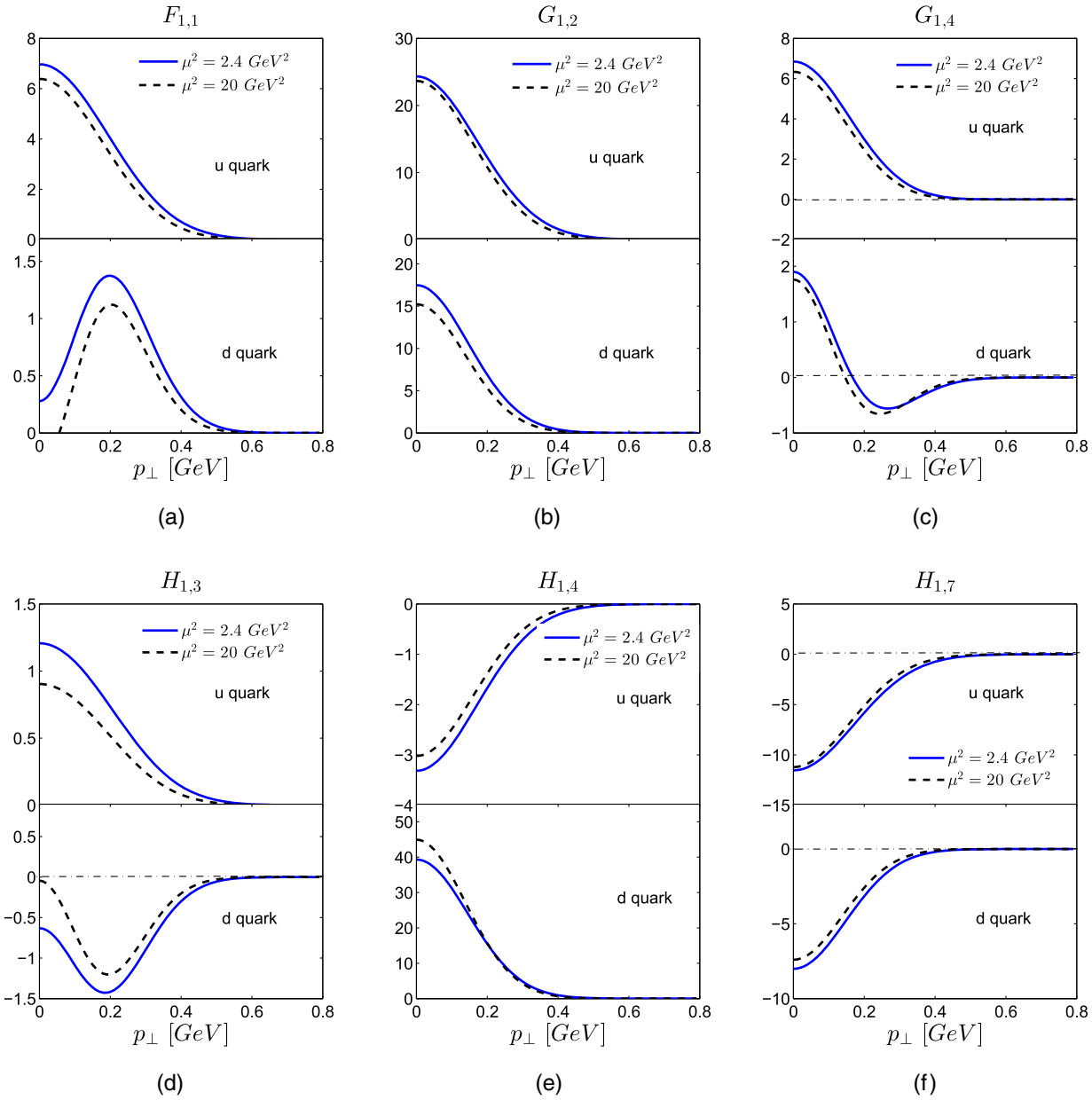

FIG. 16. Scale evolution of GTMDs with $x = 0.3$ and $\Delta_\perp^2 = 0.1$ GeV^2 for u and d quarks. The continuous lines are at $\mu^2 = 2.4$ GeV^2 (the average μ^2 value of the HERMES experiment), and the dotted lines are at $\mu^2 = 20$ GeV^2 (the highest bin average μ^2 value of the COMPASS experiment).

$$H^\nu_{1,5}(x, \mathbf{\Delta}_\perp^2, \mathbf{p}_\perp^2) = 0, \tag{92}$$

$$H^\nu_{1,6}(x, \mathbf{\Delta}_\perp^2, \mathbf{p}_\perp^2) = N^\nu_{TT} \frac{1}{16\pi^3} \left[\frac{(1-x)^2}{2x^2} |A_2^\nu|^2\right] \exp[-2\tilde{a}(x)\tilde{\mathbf{p}}_\perp^2] + \frac{1}{2} H^\nu_{1,2}(x, \mathbf{\Delta}_\perp^2, \mathbf{p}_\perp^2), \tag{93}$$

$$H^\nu_{1,7}(x, \mathbf{\Delta}_\perp^2, \mathbf{p}_\perp^2) = N^\nu_{LT} \frac{1}{16\pi^3} \left[\frac{1}{x} A_1^\nu(x) A_2^\nu(x)\right] \exp[-2\tilde{a}(x)\tilde{\mathbf{p}}_\perp^2], \tag{94}$$

$$H^\nu_{1,8}(x, \mathbf{\Delta}_\perp^2, \mathbf{p}_\perp^2) = 0. \tag{95}$$

The normalization constants $N^{\nu}_{\Lambda\lambda}$ are

$$N^{\nu}_{UU} = \left(C_S^2 N_S^2 + C_V^2\left(\frac{1}{3}N_0^2 + \frac{2}{3}N_1^2\right)\right)^{\nu}, \qquad N^{\nu}_{LT} = \left(-C_S^2 N_S^2 - C_V^2\left(\frac{1}{3}N_0^2 - \frac{2}{3}N_1^2\right)\right)^{\nu},$$
$$N^{\nu}_{UL} = \left(-C_S^2 N_S^2 - C_V^2\left(\frac{1}{3}N_0^2 + \frac{2}{3}N_1^2\right)\right)^{\nu}, \qquad N^{\nu}_{TU} = \left(C_S^2 N_S^2 + C_V^2\frac{1}{3}N_0^2\right)^{\nu},$$
$$N^{\nu}_{UT} = \left(C_S^2 N_S^2 + C_V^2\left(\frac{1}{3}N_0^2 + \frac{2}{3}N_1^2\right)\right)^{\nu}, \qquad N^{\nu}_{TL} = \left(C_S^2 N_S^2 - C_V^2\frac{1}{3}N_0^2\right)^{\nu},$$
$$N^{\nu}_{LU} = \left(C_S^2 N_S^2 + C_V^2\left(\frac{1}{3}N_0^2 - \frac{2}{3}N_1^2\right)\right)^{\nu}, \qquad N^{\nu}_{TT} = \left(C_S^2 N_S^2 - C_V^2\frac{1}{3}N_0^2\right)^{\nu},$$
$$N^{\nu}_{LL} = \left(C_S^2 N_S^2 + C_V^2\left(\frac{1}{3}N_0^2 - \frac{2}{3}N_1^2\right)\right)^{\nu}, \qquad N^{\perp\nu}_{TT} = \left(-C_S^2 N_S^2 + C_V^2\frac{1}{3}N_0^2\right)^{\nu}, \tag{96}$$

where $N_S = 0$ for the d quark.

The scale evolution of the GTMDs is modeled by considering the evolution of the parameters that reproduce the correct scale evolution of the PDFs [18]. The LFWFs are defined at the initial scale $\mu_0 = 0.313$ GeV, and the hard scale evolution of the distributions are modeled by making the parameters in the distribution scale dependent. The scale evolution of the parameters is determined by the DGLAP evolution of the PDFs:

$$a^{\nu}_i(\mu) = a^{\nu}_i(\mu_0) + A^{\nu}_i(\mu), \tag{97}$$

$$b^{\nu}_i(\mu) = b^{\nu}_i(\mu_0) - B^{\nu}_i(\mu)\frac{4C_F}{\beta_0}\ln\left(\frac{\alpha_s(\mu^2)}{\alpha_s(\mu_0^2)}\right), \tag{98}$$

$$\delta^{\nu}(\mu) = \exp[\delta^{\nu}_1(\ln(\mu^2/\mu_0^2))^{\delta^{\nu}_2}], \tag{99}$$

where $a^{\nu}_i(\mu_0)$ and $b^{\nu}_i(\mu_0)$ are the parameters at $\mu = \mu_0$. The parameter δ^{ν} becomes unity at μ_0 for both u and d quarks. The scale-dependent parts $A^{\nu}_i(\mu)$ and $B^{\nu}_i(\mu)$ evolve as

$$P^{\nu}_i(\mu) = \alpha^{\nu}_{P,i}\mu^{2\beta^{\nu}_{P,i}}\left[\ln\left(\frac{\mu^2}{\mu_0^2}\right)\right]^{\gamma^{\nu}_{P,i}}\Bigg|_{i=1,2}, \tag{100}$$

where the subscript P on the right-hand side of the above equation stands for $P = A, B$, corresponding to $P^{\nu}_i(\mu) = A^{\nu}_i(\mu), B^{\nu}_i(\mu)$, respectively. The detail of the scheme and the values of the parameters are given in Ref. [18].

Our model predictions for the GTMDs $F^{\nu}_{1,1}, G^{\nu}_{1,2}, G_{1,4^{\nu}}, H^{\nu}_{1,3}, H^{\nu}_{1,4}$ and $H^{\nu}_{1,7}$ are shown in Fig. 16 at the scale $\mu^2 = 2.4$ GeV^2, which is the average μ^2 value of the HERMES experiment, and at $\mu^2 = 20$ GeV^2, which is the highest bin average μ^2 value of the COMPASS experiment. At the TMD limit, the GTMDs $F^{\nu}_{1,1}, G^{\nu}_{1,2}, G^{\nu}_{1,4}, H^{\nu}_{1,3}, H^{\nu}_{1,4}$ and $H^{\nu}_{1,7}$ give the leading-twist TMDs $f^{\nu}_1, g^{\nu}_{1T}, g^{\nu}_{1L}, h^{\nu}_{1T}$ and $h^{\perp\nu}_{1L}$, respectively. We plot the GTMDs for $x = 0.3$ and $\mathbf{\Delta}^2_\perp = 0.1$ GeV^2. We notice that the GTMD $G_{1,4}$ for the d quark approaches negative values at higher scales. This causes a negative axial charge for the d quark, as found experimentally. The scale evolution of GTMDs is considered in Ref. [5] and shown to be the same as for TMDs.

VII. INEQUALITIES

It is interesting to express the transverse GTMDs in terms of the unpolarized and longitudinal GTMDs at the leading twist. Some inequality relations for GTMDs with $\mathbf{p}^2_\perp > \frac{\mathbf{\Delta}^2_\perp}{4}(1-x)^2$ found in this model are

$$|H^{\nu}_{1,3}(x,\mathbf{\Delta}^2_\perp,\mathbf{p}^2_\perp) + \frac{\mathbf{p}^2_\perp}{2M^2}H^{\nu}_{1,4}(x,\mathbf{\Delta}^2_\perp,\mathbf{p}^2_\perp)| < \frac{1}{2}|F^{\nu}_{1,1}(x,\mathbf{\Delta}^2_\perp,\mathbf{p}^2_\perp) + G^{\nu}_{1,4}(x,\mathbf{\Delta}^2_\perp,\mathbf{p}^2_\perp)|, \tag{101}$$

$$|F^{\nu}_{1,1}(x,\mathbf{\Delta}^2_\perp,\mathbf{p}^2_\perp)| > |H^{\nu}_{1,3}(x,\mathbf{\Delta}^2_\perp,\mathbf{p}^2_\perp) + \frac{\mathbf{p}^2_\perp}{2M^2}H^{\nu}_{1,4}(x,\mathbf{\Delta}^2_\perp,\mathbf{p}^2_\perp)|, \tag{102}$$

$$|F^{\nu}_{1,1}(x,\mathbf{\Delta}^2_\perp,\mathbf{p}^2_\perp)| > |H^{\nu}_{1,3}(x,\mathbf{\Delta}^2_\perp,\mathbf{p}^2_\perp)|, \tag{103}$$

$$F^{\nu}_{1,1}(x,\mathbf{\Delta}^2_\perp,\mathbf{p}^2_\perp) > 0, \tag{104}$$

$$F^{\nu}_{1,1}(x,\mathbf{\Delta}^2_\perp,\mathbf{p}^2_\perp) > G^{\nu}_{1,4}(x,\mathbf{\Delta}^2_\perp,\mathbf{p}^2_\perp), \tag{105}$$

$$\frac{\mathbf{p}^2_\perp}{2M^2}|H^{\nu}_{1,4}(x,\mathbf{\Delta}^2_\perp,\mathbf{p}^2_\perp)| < \frac{1}{2}|F^{\nu}_{1,1}(x,\mathbf{\Delta}^2_\perp,\mathbf{p}^2_\perp) + G^{\nu}_{1,4}(x,\mathbf{\Delta}^2_\perp,\mathbf{p}^2_\perp)|. \tag{106}$$

Equation (101) represents the Soffer bound [28] for GTMDs. We observe that at the TMD limit, i.e. at $\mathbf{\Delta}_\perp = 0$, the above relations reduce to the relations discussed in Ref. [29] for the light-front quark-scalar-diquark model.

We can also find some inequalities for Wigner distributions given by

$$\rho^{\nu}_{UU}(\mathbf{b}_\perp, \mathbf{p}_\perp, x) > 0, \tag{107}$$

$$\rho^{\nu}_{UU}(\mathbf{b}_\perp, \mathbf{p}_\perp, x) > \rho^{\nu}_{LL}(\mathbf{b}_\perp, \mathbf{p}_\perp, x), \tag{108}$$

$$\rho^{\nu}_{TT}(\mathbf{b}_\perp, \mathbf{p}_\perp, x) < \frac{1}{2}[\rho^{\nu}_{UU}(\mathbf{b}_\perp, \mathbf{p}_\perp, x) + \rho^{\nu}_{LL}(\mathbf{b}_\perp, \mathbf{p}_\perp, x)]. \tag{109}$$

Equation (109) can be regarded as a generalized Soffer bound for the Wigner distributions. It will be interesting to check if other models also satisfy similar inequalities.

VIII. CONCLUSIONS

We calculated the Wigner distributions of quarks in a nucleon using a diquark model. The light-front wave functions are modeled using ADS/QCD predictions. We examined both scalar and vector diquarks [18]. We have presented results of the Wigner distributions in transverse position and momentum space as well as mixed position and momentum space for unpolarized, longitudinally polarized, and transversely polarized quarks and protons and compared them with other model predictions. We have noted a few inequalities among ρ_{UU}, ρ_{LL} and ρ_{TT} in this model. It will be interesting to check if such inequalities are present in other models, particularly in models with gluonic degrees of freedom. The scale evolutions of the parton distribution functions are modeled by making the parameters scale dependent in accord with DGLAP equation. We have used the same evolution of the parameters in our calculation for the GTMDs. Relations of the Wigner distributions and GTMDs with the quark orbital angular momentum and spin-spin correlations are discussed.

ACKNOWLEDGMENTS

We thank Oleg Teryaev for many useful discussions.

[1] X. Ji, Phys. Rev. Lett. **91**, 062001 (2003).
[2] A. V. Belitsky, X. Ji, and F. Yuan, Phys. Rev. D **69**, 074014 (2004).
[3] S. Meissner, A. Metz, M. Schlegel, and K. Goeke, J. High Energy Phys. 08 (2008) 038.
[4] S. Meissner, A. Metz, and M. Schlegel, J. High Energy Phys. 08 (2009) 056.
[5] M. G. Echevarria, A. Idilbi, K. Kanazawa, C. Lorc, A. Metz, B. Pasquini, and M. Schlegel, Phys. Lett. B **759**, 336 (2016).
[6] C. Lorc and B. Pasquini, J. High Energy Phys. 09 (2013) 138.
[7] C. Lorce, B. Pasquini, X. Xiong, and F. Yuan, Phys. Rev. D **85**, 114006 (2012).
[8] C. Lorce and B. Pasquini, Phys. Rev. D **84**, 014015 (2011).
[9] S. Boffi, B. Pasquini, and M. Traini, Nucl. Phys. **B649**, 243 (2003).
[10] S. Boffi, B. Pasquini, and M. Traini, Nucl. Phys. **B680**, 147 (2004).
[11] C. Lorce, Phys. Rev. D **74**, 054019 (2006); **78**, 034001 (2008); **79**, 074027 (2009).
[12] D. Diakonov and V. Petrov, Phys. Rev. D **72**, 074009 (2005).
[13] A. Mukherjee, S. Nair, and V. K. Ojha, Phys. Rev. D **90**, 014024 (2014).
[14] A. Mukherjee, S. Nair, and V. K. Ojha, Phys. Rev. D **91**, 054018 (2015).
[15] J. More, A. Mukherjee, and S. Nair, arXiv:1701.00339.
[16] Tianbo Liu and Bo-Qiang Ma, Phys. Rev. D **91**, 034019 (2015).
[17] D. Chakrabarti, T. Maji, C. Mondal, and A. Mukherjee, Eur. Phys. J. C **76**, 409 (2016).
[18] T. Maji and D. Chakrabarti, Phys. Rev. D **94**, 094020 (2016).
[19] R. Jakob, P. J. Mulders, and J. Rodrigues, Nucl. Phys. **A626**, 937 (1997).
[20] A. Bacchetta, F. Conti, and M. Radici, Phys. Rev. D **78**, 074010 (2008).
[21] G. P. Lepage and S. J. Brodsky, Phys. Rev. D **22**, 2157 (1980).
[22] J. R. Ellis, D. S. Hwang, and A. Kotzinian, Phys. Rev. D **80**, 074033 (2009).
[23] S. J. Brodsky and G. F. de Teramond, Phys. Rev. D **77**, 056007 (2008).
[24] G. F. de Teramond and S. J. Brodsky, arXiv:1203.4025.
[25] D. Chakrabarti and C. Mondal, Phys. Rev. D **88**, 073006 (2013); Eur. Phys. J. C **73**, 2671 (2013).
[26] T. Liu and B. Q. Ma, Phys. Rev. D **91**, 034019 (2015).
[27] A. Courtoy and A. S. Miramontes, Phys. Rev. D **95**, 014027 (2017).
[28] J. Soffer, Phys. Rev. Lett. **74**, 1292 (1995).
[29] T. Maji, C. Mondal, D. Chakrabarti, and O. V. Teryaev, J. High Energy Phys. 01 (2016) 165.